

# Chemical characterization and source apportionment of submicron aerosols measured in Senegal during the 2015 SHADOW campaign

Laura-Hélène Rivellini<sup>1,2,\*</sup>, Isabelle Chiapello<sup>2</sup>, Emmanuel Tison<sup>1</sup>, Marc Fourmentin<sup>3</sup>, Anaïs Féron<sup>4</sup>, Aboubacry Diallo<sup>5</sup>, Thierno N'Diaye<sup>5</sup>, Philippe Goloub<sup>2</sup>, Francesco Canonaco<sup>6</sup>, André Stephan Henry Prévôt<sup>6</sup>, and Véronique Riffault<sup>1,\*</sup>

<sup>1</sup>IMT Lille Douai, Univ. Lille, SAGE - Département Sciences de l'Atmosphère et Génie de l'Environnement, 59000 Lille, France

<sup>2</sup>Univ. Lille, CNRS, UMR8518 – LOA – Laboratoire d'Optique Atmosphérique, F-59000 Lille, France

<sup>3</sup>Laboratoire de Physico-Chimie de l'Atmosphère, Université du Littoral Côte d'Opale, Dunkerque, 59140, France

<sup>4</sup>Laboratoire Interuniversitaire des Systèmes Atmosphériques, CNRS - Université Paris Est Créteil - Université Paris Diderot, Créteil, 94010, France

<sup>5</sup>Institut de Recherche pour le Développement, M'Bour, Senegal

<sup>6</sup>Laboratory of Atmospheric Chemistry, Paul Scherrer Institute, 5232 Villigen, Switzerland

\* Correspondence to:

Véronique Riffault

Tel.: +33 327 712 604, Fax: +33 327 712 914, e-mail: [veronique.riffault@imt-lille-douai.fr](mailto:veronique.riffault@imt-lille-douai.fr)

Laura-Hélène Rivellini

e-mail: [laura.rivellini@imt-lille-douai.fr](mailto:laura.rivellini@imt-lille-douai.fr)

**Abstract.** The present study offers the first chemical characterization of the submicron (PM<sub>1</sub>) fraction in West Africa at a high time resolution, thanks to collocated measurements of non-refractory (NR) species with an Aerosol Chemical Speciation Monitor (ACSM), black carbon and iron concentrations derived from absorption coefficient measurements with a 7-wavelength aethalometer, and total PM<sub>1</sub> determined by a TEOM-FDMS for mass closure. The field campaign was carried out during three months (March to June 2015) as part of the SHADOW (SaHaran Dust Over West Africa) project at a coastal site located in the outskirts of the city of M'Bour, Senegal. With an averaged mass concentration of 5.4 µg m<sup>-3</sup>, levels of NR-PM<sub>1</sub> in M'Bour were three to ten times lower than those generally measured in urban and suburban polluted environments. Nonetheless the first half of the observation period was marked by intense but short pollution events (NR-PM<sub>1</sub> concentrations higher than 15 µg m<sup>-3</sup>), sea breeze phenomena and Saharan desert dust outbreaks (PM<sub>10</sub> up to 900 µg m<sup>-3</sup>). During the second half of the campaign, the sampling site was mainly under the influence of marine air masses. The air masses on days under continental and sea breeze influences were dominated by organics (36-40%), whereas sulfate particles were predominant (40%) for days under oceanic influence. Overall, measurements showed that about 3/4 of the total PM<sub>1</sub> were explained by NR-PM<sub>1</sub>, BC and Fe (a proxy for dust) concentrations, leaving ~1/4 for other refractory species. A mean value of 4.6% for the Fe/PM<sub>1</sub> ratio was obtained. Source apportionment of the organic fraction, using Positive Matrix Factorization (PMF) highlighted the impact of local combustion sources, such as traffic and residential activities, which contribute on

average to 52% of the total organic fraction. A new organic aerosol (OA) source, representing on average 3% of the total OA fraction, showed similar variation as non-refractory particulate chloride. Its rose plot and daily pattern pointed out to local combustion processes, that is to say two open waste burning areas located about 6 and 11 km away from the receptor site and to a lesser extent a traditional fish smoking place. The remaining fraction was identified as oxygenated organic aerosols (OOA), a factor that prevailed regardless of the day type (45%) and was representative of regional ( $\sim 3/4$ ) but also local ( $\sim 1/4$ ) sources due to enhanced photochemical processes.

## 1 Introduction

Atmospheric aerosols play a key role in the Earth's radiative forcing, by interacting with incoming solar and outgoing terrestrial radiations (direct effect) and influencing cloud formation, growth and lifetime (indirect effects). Important uncertainties related to such effects remain, as reported in the IPCC reports (IPCC, 2007, 2013). Besides, several epidemiological and toxicological studies (Brook et al., 2004; Kelly and Fussell, 2012) also highlight the sanitary impacts of particulate matter (PM) depending on their size, chemical composition and exposure time. In 2012, around 3.7 million deaths were attributed to cardiovascular and respiratory diseases caused by outdoor PM exposure (Brauer et al., 2012). As a response, the World Health Organization (WHO) established in 2006 air quality thresholds for PM: a daily average of 25 (respectively 50)  $\mu\text{g m}^{-3}$  and a mean annual limit of 10 (respectively 20)  $\mu\text{g m}^{-3}$  for  $\text{PM}_{2.5}$  (PM with diameter  $< 2.5 \mu\text{m}$ ) ( $\text{PM}_{10}$ ) (WHO, 2006). During past decades, high-time resolution monitoring instruments have been implemented in Europe within the ACTRIS (Aerosols, Clouds, and Trace gases Research Infrastructure network) program, in America with the IMPROVE (Interagency Monitoring of Protected Visual Environments) network (Prenni et al., 2016; Schurman et al., 2015) or more recently in Asia, in order to better characterize fine particles. Yet, the African continent remains poorly documented in terms of particulate pollution.

Several studies in West Africa (mostly sub-Saharan regions) have focused on the coarse fraction, since this area is strongly influenced by natural sources, especially the Sahara desert that injects high amounts of mineral aerosols into the atmosphere (e.g Chiapello et al., 1995). Among field campaigns, a large effort was performed on aerosol measurements during the AMMA (African Monsoon Multidisciplinary Analysis) program carried out between 2002 and 2010, with intensive observation periods in 2006 (Redelsperger et al., 2006). During the months of January-February (dry season) the transport of desert dust (DD) and biomass burning (BB) aerosols were observed to occur into two layers, one dominated by DD close to the surface ( $< 1 \text{ km}$ ), the one containing BB aerosols being located at a higher altitude, between 2 and 4 km (Haywood et al., 2008; Osborne et al., 2008). During one of the AMMA special observing periods (SOP) (February 2006), a chemical characterization of particles at the ground level was performed near M'Bour (Senegal) using filter sampling and individual particle analysis (Deboudt et al., 2010; Flament et al., 2011). The analysis evidenced both internal and external mixing of DD, sea salt (SS) and carbonaceous aerosols (Deboudt et al., 2010) within the surface layer. The compositions of the coarse (2-10  $\mu\text{m}$ ) and fine ( $< 2 \mu\text{m}$ ) fractions were established at the surface; DD dominated the coarse fraction while organic matter was the major constituent of the fine one. Similar analysis were performed on samples collected during aircraft flights (Formenti et al., 2008a) to determine the chemical composition of aerosols at different altitudes. The altitude layer

was mainly composed of BB and DD external mixture (Chou et al., 2008; Hand et al., 2010). From January to March 2006 (AMMA SOP-0), several types of events from mixtures of DD and BB aerosols to pure mineral dust events were identified based on column aerosol retrievals from AERONET sun/sky photometer measurements in M'Bour, Senegal (Derimian et al., 2008). Other field campaigns such as POLCA ("POLlution des Capitales Africaines" on the Pollution of African Capitals) highlighted the presence of anthropogenic sources of aerosols linked to the strong demographic growth, limited traffic pollution regulations and traditional activities such as slash-and-burn cultivation that generates huge amounts of BB aerosols (Liousse et al., 2010). Its aim was rather on the chemical characterization of PM<sub>2.5</sub>, especially Black Carbon (Doumbia et al., 2012), and the impact on health (Val et al., 2013). Nevertheless, to the best of our knowledge, only one other study has performed on-line and real-time chemical characterization of major PM<sub>1</sub> constituents on the African continent. It was conducted during one year in Welgegund, South Africa, at a site influenced by anthropogenic sources and devoid of mineral dust or marine contribution (Tiitta et al., 2014). Their results have shown that the submicron fraction was dominated by organic and sulfate species, with a chemical composition similar to those encountered in megacities like Beijing (Sun et al., 2012), Mexico (Salcedo et al., 2006) or Pittsburgh (Zhang et al., 2005). Such a pattern differs strongly from those recently measured in European urban cities, where the main submicron pollutants are organic and nitrate species (Petit et al., 2015; Schlag et al., 2015).

In this study we offer the first insight of a real-time, continuous and long-term chemical characterization of PM<sub>1</sub> in West Africa, performed in M'Bour, Senegal from March to June 2015 as part of the first intensive observation period (IOP-1) of the SHADOW (SaHaran Dust Over West Africa) field campaign. An Aerosol Chemical Speciation Monitor (ACSM) was chosen for the quantification and chemical characterization of non-refractory submicron particles, the instrument being better suited for unattended and long term monitoring. Parallel measurements of BC and total PM<sub>1</sub> allowed for mass closure. This paper reports the chemical composition of the submicron fraction and the temporal behaviour of particulate species. The sources and processes responsible for the concentrations encountered at the M'Bour site over the period have been assessed using source-receptor modeling as well as dynamic meteorological measurements parameters and back-trajectory analyses.

## 2 Instrumentation and methods

### 2.1 Site description and the SHADOW campaign

The sampling site is located within the '*Institut de Recherche et Développement*' (IRD) facility in M'Bour (14°23'38"N, 16°57'32"W), Senegal. This site, located near the seashore at 80 km south of Dakar (Figure 1), is known to be under the influence of Saharan dust, sea salt, and biomass burning during part of the dry season. The site may also be affected by regional anthropogenic emissions from surrounding cities including M'Bour and Dakar, and from traditional fish-smoking activities and open waste burning areas. These potential aerosol source locations are reported in Figure 1. The M'Bour station, as part of the international AERONET network (Holben et al., 1998) is routinely equipped with active and passive remote sensing instruments for cloud, aerosol and meteorological monitoring (CIMEL sun/sky photometer, CIMEL micro-Lidar, fluxmeters and a weather station). Since the AMMA

campaigns in 2006, M'Bour is also one of the three ground-based stations of the "Sahelian Dust Transect" where  $PM_{10}$  mass concentrations are measured continuously (every 5 minutes) thanks to a Tapered Element Oscillating Microbalance (TEOM) (Marticorena et al., 2010; Kaly et al., 2015).

SHADOW main objectives are to better determine the physical and chemical properties of particles in this region largely influenced by high concentrations, and to establish a link between them, the atmospheric dynamics and the aerosol load and optical properties. A large panel of high-performance instruments has therefore been added to the AERONET station (Holben et al., 1998) implemented in M'Bour since 1996 (Derimian et al., 2008). Optical and microphysical aerosol measurements (results not presented) were also performed on site by active and passive remote-sensing instruments, like the LiLAS LIDAR (Bovchaliuk et al., 2014; Veselovskii et al., 2016) and a PLASMA airborne sun photometer (Karol et al., 2013).  $PM_{10}$  in situ optical measurements at the surface were carried out by a mono-wavelength aethalometer and a nephelometer. Fine and coarse particle size distributions were recorded by a GRIMM optical particle counter, while ground and airborne filter sampling were collected through a 4-stage DEKATI cascade impactor to be analyzed off-line by individual particle analysis. A Doppler Lidar was implemented to improve our understanding of the atmospheric dynamics between the surface and up to 2-3 km over the IRD station in order to provide more accurate micro-meteorological information.

The online chemical composition measurements presented here were acquired during IOP-1, which took place from March 20 to June 22, 2015. Results discussed in this paper focus on the chemical characterization of surface  $PM_{10}$ . The instruments presented hereafter were set up in an air-conditioned room located underneath the flat roof of the IRD main building. Co-located wind speed and direction were measured by an ultrasonic anemometer (model USA-1, METEK GmbH) deployed on the rooftop (about 12 m above ground).

## 2.2 Instrumentation

### 2.2.1 ACSM

The chemical characterization of non-refractory submicron particles (NR- $PM_{10}$ ), that is to say material vaporizing around 600°C under close-to-vacuum conditions, was performed on-line and in real time every 30 minutes by an ACSM (Aerodyne Research Inc.). This instrument is based on the same principle as the aerosol mass spectrometers (AMS), without providing size distribution information. A full description of the instrument is presented in Ng et al. (2011). Basically it is composed of an aerodynamic lens that focuses the particle beam (with vacuum aerodynamic diameters below 1  $\mu m$ ) and directs it through three vacuum chambers, the last one being a detection chamber in which particles are vaporized by impaction on a surface heated at 600°C. Non-refractory species, such as organic matter (OM), sulfate ( $SO_4$ ), nitrate ( $NO_3$ ), ammonium ( $NH_4$ ) and non-refractory chloride (Chl), are vaporized at this temperature and then ionized by electron impact (70 eV). The above mentioned names of the different NR species correspond to the sum of all  $m/z$  fragments related to one given species in the fragmentation table (Allan et al., 2004), that is to say  $H_{0 \leq x \leq 2}S_{0 \leq y \leq 1}O_{0 \leq z \leq 4}$  for sulfate,  $NH_{0 \leq x \leq 2}$  for ammonium,  $NO_{0 \leq x \leq 2}$  and  $HNO_3$  for nitrate, and  $H_{0 \leq x \leq 1}Cl$  for chloride.. Particles are then detected by mass spectrometry thanks to a residual gas analyser (RGA). Because of a simplest operating system and the use of a quadrupole mass spectrometer, the instrument has lower time-resolution and sensitivity but remains better suited for long-term monitoring. A  $PM_{2.5}$  cut-off inlet (URG

Cyclone 2000-30EH, Chapel Hill, NC, USA) was placed on the roof at the entrance of the sampling line with a primary flow of 3 LPM and vertically connected to the instrument. A Nafion dryer (PD-200T-12 MPS, Perma Pure) upstream of the inlet reduces the sample relative humidity (RH). Particle losses were evaluated using the Particle Loss calculator (Von der Weiden et al., 2009) and were inferior to 2% between 50 nm and 1  $\mu\text{m}$ .

Several calibrations were performed with ammonium nitrate, ammonium sulfate and ammonium chloride individual solutions (at 0.005 mol L<sup>-1</sup> in purified water) prior to IOP-1. An average of all previous calibrations with this instrument gives a mean NO<sub>3</sub> response factor (RF) of  $3.63 \times 10^{-11}$  and mean relative ionization efficiencies (RIE) of 5.72, 0.58 and 2.26 for ammonium, sulfate and chloride, respectively (see Supplementary Information S1 – Figure S1(a-e) and Zhang et al., in prep., for more details). Organic and nitrate RIE default values of 1.4 and 1.1, respectively, were used (Canagaratna et al., 2007). Detection limits in  $\mu\text{g m}^{-3}$  were determined by Ng et al. (2011) to be 0.284 for ammonium, 0.148 for organic matter, 0.024 for sulfate, 0.012 for nitrate and 0.011 for chloride. It must be noted however that the uncertainties on mass concentrations with aerosol mass spectrometers are estimated at 20–35% (2 $\sigma$ ) for the total mass (Bahreini et al., 2009). Furthermore, Crenn et al. (2015) reported reproducibility expanded uncertainties of Q-ACSM concentration measurements of 9, 15, 19, 28, and 36% for NR-PM<sub>1</sub>, nitrate, organic matter, sulfate, and ammonium, respectively, during an intercomparison that involved 13 Q-ACSM in the Paris area during springtime. In addition to the relative ion transmission efficiency correction applied using a naphthalene internal standard, the Collection Efficiency (CE) due to particle losses induced by an incomplete vaporization and/or transmission through the aerodynamic lens was also determined for the whole dataset. Those parameters are mainly influenced by particle shape (size, sphericity) and acidity, ammonium nitrate fraction and RH in the sampling line. Middlebrook et al. (2012) have developed a correction algorithm based on AMS datasets which is applied on ACSM mass concentrations and which considers both RH and aerosol chemical composition to obtain a time-dependent correction of CE values ranging from 0.45 to 0.83 (Figure S1f). Nonetheless due to the presence of the Nafion dryer at the entrance of the instrument no RH corrections were necessary as RH values were below 30%. A minor fraction (3.2%) of the data was excluded from the dataset due to unstable parameters, which were generally observed after restarting the instrument following power outages.

### 2.2.2 AE33 aethalometer

Real-time measurements of aerosol absorption were performed every minute by a seven-wavelength (370, 470, 520, 590, 660, 880 and 950 nm) aethalometer (AE33, Magee Scientific Inc.). The instrument was equipped with a PM<sub>1</sub> impactor inlet (BGI model SCC-0.732, Waltham, MA, USA) and sampled at 5 L min<sup>-1</sup>. The aethalometer principle is based on the measurement of light transmission through a filter onto which aerosols deposit. The attenuation is then converted into an aerosol absorption coefficient  $\sigma_{aer}$  for each wavelength. BC concentrations are retrieved by applying a specific mass absorption cross section of 7.77 m<sup>2</sup> g<sup>-1</sup> to the absorption coefficient at 880 nm. The AE33 instrument uses internal corrections based on the Weingartner et al. (2003) algorithm to account for multiple scattering by the filter and a dual spot technology (Drinovec et al., 2015) to compensate the loading effect. Even if DD absorption is limited at 880 nm, its occurrence in high concentrations on site might cause an overestimation of BC concentrations derived from absorption measurements. The method developed by Fialho et al. (2005, 2006,

2014) was used to correct BC concentration data from mineral dust interference. This method is further explained in section II.3.2.

### 2.2.3 Other instruments

To achieve mass closure in the submicron fraction and account for the expected refractory material (mineral dust and sea salt), ambient air was sampled at  $16.7 \text{ L min}^{-1}$  through a  $\text{PM}_{10}$ -inlet (Thermo Fisher Scientific Inc.) mounted on a  $\text{PM}_1$  cyclone (SCC 2.229, BGI Inc., Waltham, MA). Gravimetric measurements of the total mass concentrations were performed every 6 minutes using a TEOM operating at a temperature of  $30^\circ\text{C}$  and equipped with a filtered dynamic measurement system (TEOM-FDMS 1405-F, Thermo Scientific) that can account for semi-volatile material by maintaining temperature under  $30^\circ\text{C}$  and relative humidity (RH) below 25 %, as described by Grover et al. (2005). Some data had to be discarded, mainly due to high temperatures encountered during dust events leading to FDMS failure to maintain proper operating conditions.

Micro-meteorological parameters (wind speed and direction) at the surface ( $\sim 10 \text{ m}$  high) were obtained from 15-minutes accumulation (at  $20 \text{ Hz}$ ) with an ultrasonic anemometer (model USA-1 by METEK GmbH) with a resolution of  $0.01 \text{ m s}^{-1}$  and  $1^\circ$ , respectively. A weather station (Campbell Scientific) provided precipitation, RH and temperature data every 10 min.

## 2.3 Analysis strategy

### 2.3.1 Classification of air masses

The station of M'Bour is under the influence of a typical Sahelian climatic cycle composed of two contrasted dry and wet seasons observed around the Equator, which originate from the closeness of the Intertropical Convergence Zone (ITCZ), bringing moist air masses and heavy precipitations. Kaly et al. (2015), based on 5 years of observations (2006-2010) at M'Bour, defined the dry season as the period during which no precipitation occurs from November to April and the wet season from May to October, where significant precipitation is measured, with a transition during April/May. In Mortier et al. (2016), who analyzed data from 2006 to 2012 at M'Bour, the seasons are defined based on RH levels: from December to March/April ( $\text{RH} < 40\%$ ) for the dry season and from June to September ( $\text{RH} \sim 80\%$ ) for the wet season. They also observed different wind patterns at the ground level, that is to say trade winds coming mostly from the North-East during the dry season, whereas the wet season was characterized by winds from the west. During the AMMA field campaign in the Sahelian belt, Haywood et al. (2008) defined the period from May to June as the monsoon onset. Finally, Slingo et al. (2008) also mentioned large inter-annual variability in the seasonal progression of moisture, with no clearly reproducible pattern from year-to-year in Niamey, Niger.

Therefore we based the definition of the dry and wet seasons in this work on the observed weather parameters during the field campaign. Since absolutely no precipitation was observed during the whole period, but differences in RH levels – though not as pronounced as reported by Mortier et al. (2016) – and wind patterns were clearly visible (Figure 2a), we considered March ( $\text{RH} = 49\%$ ) and April ( $68\%$ ) to belong to the dry season, and May ( $82\%$ ) and June ( $84\%$ ) to the transition period.

During IOP-1 two main prevailing directions were found (Fig. 2a). The first one corresponds to an oceanic influence characterized by surface winds coming from West-South-West to North-West (210-300°) with a total frequency of 56% and wind speeds between 2 and 4 m s<sup>-1</sup>. The second predominant direction is observed for winds originating from NW to NE (300 to 60°) with a total frequency of around 42% and similar wind speeds (2-4 m s<sup>-1</sup>). The remaining wind sector (60-210°) is a negligible fraction (2%) (Fig. 2a). The maximum wind speed, 6.8 m s<sup>-1</sup>, was measured on June 21, 2015, with values above 6 m s<sup>-1</sup> recorded between 2 and 6 a.m. and associated to SW direction. The period from end of March to April was dominated by winds coming from NW to NE (~62%) with some occurrences (~33%) of Western winds during the sea breezes, while from May to June winds were mainly originating from the West (72%).

Our measurements during IOP-1 are generally consistent with monthly average frequencies of M'Bour surface wind directions reported by Kaly et al. (2015) between 2006 and 2010. Indeed, their climatology has shown that spring months are generally influenced by winds coming predominantly from two main sectors, North to East (0-90°, prevailing in March-April) and North-West to South-West (315-225°, dominant in May-June).

Each sampling day of IOP-1 was classified according to the locally measured surface wind directions. Three categories of days were indeed identified: (i) days exclusively under northern (N) trade wind influences, i.e. within ± 45° of the North (0°) direction, associated with continental influence, have been defined as “continental” (Fig. 2b); (ii) days dominated by westerly winds corresponding to oceanic air masses have been classified as “marine” days (Fig. 2b); (iii) an intermediate category called “sea breeze” days has been observed during which measurements show winds coming from the NE before 2 pm, then shifting from the N to W directions between 2 and 7 pm, and returning to the NW in the evening (Fig. 2b). This phenomenon has been previously observed in M'Bour during the AMMA campaigns as reported by Derimian et al. (2008), Léon et al. (2009) and Deboudt et al. (2012). In summary, among the 91 days of IOP-1, 19% were classified as continental days, 32% as sea breeze days and 49% as marine days. The frequent occurrence of marine days can be explained by the transition from dry to wet season from April to June in the Sahelian region (Redelsperger et al., 2006; Slingo et al., 2008).

### 2.3.2 Interpretation of absorption measurements

M'Bour being largely under the influence of mineral dust, a possible overestimation of the amount of BC derived from absorption coefficients measured by the aethalometer (due to DD absorbing properties at shorter wavelengths) has to be considered (Bond and Bergstrom, 2006). These interferences may be enhanced during the dry season by internal mixture of BB and DD, as encountered and evidenced during AMMA by Deboudt et al. (2010) at the surface and by Hand et al. (2010) and Paris et al. (2010) at higher altitude. Consequently, BC absorption coefficients have been recalculated following the method developed by Fialho et al. (2005, 2006, 2014) in order to obtain BC concentrations unbiased by DD influence. It consists in a deconvolution of the wavelength-dependent aerosol absorption coefficient over time,  $\sigma_{aer}(\lambda, t)$ , into two terms that take into account DD and BC contributions, through the following equations:

$$\sigma_{aer}(\lambda, t) = \sigma_{BC}(\lambda, t) + \sigma_{DD}(\lambda, t) \quad (1)$$

where  $\sigma_{BC}(\lambda, t)$  and  $\sigma_{DD}(\lambda, t)$  are BC and DD absorption coefficients, respectively, which can be expressed as a function of the species concentrations  $\langle C_i(t) \rangle$ :

$$\sigma_{BC}(\lambda, t) = K_{BC} \lambda^{\alpha} \langle C_{BC}(t) \rangle \quad (2)$$

$$\sigma_{DD}(\lambda, t) = K_{DD} \lambda^{\beta} \langle C_{DD}(t) \rangle \quad (3)$$

5  $K_{BC}$  and  $K_{DD}$  are empirical constants depending of instrument characteristics, and  $\alpha$  and  $\beta$  are respectively BC and DD absorption exponents.  $\alpha$  and  $\beta$  values of -1 and -4, respectively, have been determined in the visible range (from 470 to 660 nm) by Fialho et al. (2014) with a dataset acquired in the Cape Verde Islands located at approximately 500 km from our sampling site.

Fialho et al. (2006) have replaced dust by iron in order to calculate an iron concentration from dust absorption:

$$10 \quad K_{Fe} \langle C_{Fe}(t) \rangle = K_{DD} \langle C_{DD}(t) \rangle \quad (4)$$

Indeed, DD absorption is known to be mainly influenced by the iron content (Lafon et al., 2006) even if this element presents rather low mass contribution to the mineral dust total mass. As mentioned by Fialho et al. (2014), this method allows to estimate elemental iron concentrations only in the absence of brown carbon since an absorption Angström exponent of 1 (which correspond to fossil fuel BC) is applied. Therefore, other methods, such as the one  
15 proposed by Sandradewi et al. (2008) to deconvolve BC from fossil fuel and biomass burning, cannot be used in our conditions. The  $m/z$  60 signal ( $C_2H_4O_2^+$ , fragment characteristic of levoglucosan from biomass burning) was mostly absent of the ACSM dataset during IOP-1, representing on average only 0.003 (0.007 and 0.012 for the 95<sup>th</sup> and 99<sup>th</sup> percentiles, respectively, see Figure S7) of the total OM, which is identical to the threshold value of 0.3% suggested by Cubison et al. (2011) to assess the presence of BB aerosols. This point is discussed further in the source  
20 apportionment results, in which we tend to attribute  $m/z$  60 emissions to other sources. A few data points (less than 1% of the dataset), under the influence of other combustion processes from specific local activities that may cause a bias in the deconvolution algorithm, have been excluded to derive Fe concentrations (see further discussion in section III.2.2).

Combining Eq.(4) with Eq.(1, 2 and 3) leads to the following expression:

$$25 \quad \frac{\sigma_{aer}(\lambda, t)}{\lambda^{\alpha}} = K_{BC} \langle C_{BC}(t) \rangle + K_{Fe} \langle C_{Fe}(t) \rangle \lambda^{(\beta-\alpha)} \quad (5)$$

Eq. (5) can be plotted as a linear equation at each time  $t$  to determine the intercept at the origin,  $a(t)$ , and the slope,  $b(t)$ . BC and Fe concentrations are then derived using  $K_{BC} = 14.625 \mu m^2 m^2 g^{-1}$  in Eq. (6) and  $K_{Fe} = 0.234 \mu m^4 m^2 g^{-1}$  in Eq. (7), respectively:

$$\langle C_{BC}(t) \rangle = \frac{a(t)}{K_{BC}} \quad (6)$$

$$30 \quad \langle C_{Fe}(t) \rangle = \frac{b(t)}{K_{Fe}} \quad (7)$$

In the rest of the paper, when BC and Fe concentrations are mentioned, it corresponds to the deconvolved values based on the above-mentioned method.

Applying the propagation for uncertainties approach on the values of  $K_{Fe}$  (10%) and the slope  $b$  (39%, calculated using a variability of 0.2 for  $\alpha$  and  $\beta$  (Fialho et al., 2006)) gives an overall uncertainty of ~40% for iron  
35 concentrations. However the deconvolution algorithm is highly sensitive to the values of the Angström absorption exponents ( $\alpha$  and  $\beta$ ) and a more detailed discussion can be found in Appendix S2.



### 2.3.3 Positive Matrix Factorization (PMF)

The PMF model is a statistical source-receptor model developed by Paatero and Tapper (1994), largely employed in source apportionment of atmospheric pollutants when the source profiles and contributions are not known *a priori*. In this study, PMF was applied on the ACSM organic and chloride mass spectra by using the Multilinear Engine (Paatero and Tapper, 1999) and the version 5.3 of the Source Finder (SoFi) described in Canonaco et al. (2013) and operated with IgorPro 6.37 (Wavemetrics). PMF is based on a bilinear model described by the following equations:

$$X = GF + E \quad (8)$$

$$x_{ij} = \sum_{k=1}^p (g_{i,k} f_{k,j}) + e_{i,j} \quad (9)$$

where X, corresponding to model entries, represents the matrix of mass fragment spectra measured, and G and F are matrices of a *k*-factor concentration time series and *m/z* profile, respectively, where *i* denotes the time step and *j* the mass fragment. The number of factors *p* is formerly determined by the user. The residual matrix E, containing the unexplained fraction of the PMF solution, is minimized by iterations of the model using the Q function:

$$Q = \sum_i \sum_j \left( \frac{e_{ij}}{s_{ij}} \right)^2 \quad (10)$$

where *s<sub>ij</sub>* represents the measurement uncertainties of fragment *j* at time *i*. The Q value is then normalized by *Q<sub>exp</sub>*, representing the degrees of freedom of the model solution. This normalization is used as an indicator for the solution reliability. Thus a ratio *Q/Q<sub>exp</sub>* equal to one means that both variability and uncertainties are totally explained by the model. In case of mixed (known) factors, the solution can be furthermore constrained by imposing reference factor profiles (F, from the literature) as inputs. The user can apply those constraints with a certain degree of freedom defined by a scalar *a*-value ranging from 0 (no degree of freedom) up to 1 (totally unconstrained).

### 2.3.4 Geographical origins of air masses and chemical species

Air masses reaching the site were characterized through 48-hour back-trajectories (every 3 hours) retrieved from the computer version of the Hybrid Single-Particle Lagrangian Integrated Trajectory model (HYSPPLIT; Draxler and Hess (1998)), for an altitude set at one half of the mixed layer depth and coupled with the GDAS (1 degree) meteorological database. Note that sea breeze phenomena, which occur at short time and spatial scales, cannot be satisfactorily reproduced by this type of model. However given the dynamics of sea breezes, only back-trajectories arriving on site at 3 pm and eventually at 6 pm during sea breeze days (< 8.2%) could not be representative of the ground dynamic observations. Therefore all the back-trajectories available for IOP-1 were kept and could be statistically grouped into clusters according to the variation of the total spatial variance, for the whole period and also by day type.

We also used pollution roses to identify local wind directions leading to high concentrations for each species or PMF factors, but also two additional tools provided by the ZeFir Igor-based package developed by Petit et al. (2017): (i) Non-parametric regression (NWR, Henry et al. (2009)) plots, which combine smoothed surface concentrations and local wind speed and direction, to discriminate between local and more distant/regional sources; (ii) Potential Source Contribution Function (PSCF, (Polissar et al., 2001)) maps for regional sources, which couple time series of one

variable with air mass back-trajectories to redistribute the concentrations observed at the site into geographical emission parcels

### 3 Results and discussion

#### 3.1 Chemical characterization and temporal behavior

##### 5 3.1.1 NR-PM<sub>1</sub>, PM<sub>1</sub> and PM<sub>10</sub> mass concentrations

As previously mentioned, Senegal is widely influenced by DD events transported from arid and semi-arid regions of Sahara and Sahel. Moreover, M'Bour being a coastal site, the influence of sea salt (SS) particles on the measured aerosol mass concentrations may be significant. Thus, the contributions of these two aerosol types, in both the coarse and fine fractions of aerosol, have been investigated. PM<sub>1</sub> chemical mass closure was checked for all day types by  
10 subtracting from the TEOM-FDMS measurements the mass concentrations of species determined by ACSM (NR-PM<sub>1</sub>) and aethalometer (BC + Fe); the fraction of unaccounted material therefore corresponded to DD and SS contributions.

Figure 3a shows the mass concentration time series of NR-PM<sub>1</sub> measured by ACSM, total PM<sub>1</sub> by TEOM-FDMS, and PM<sub>10</sub> by TEOM during IOP-1. It must be noted that total PM<sub>1</sub> data acquired between March 28 and April 10 had  
15 to be invalidated due to instrument overheating during a dust storm event when the outside temperature reached 42°C and PM<sub>10</sub> concentrations exceeded 600 µg m<sup>-3</sup>.

The temporal evolutions of the three aerosol fractions do not show any particular correlations (the highest correlation coefficient is obtained between the PM<sub>1</sub> and PM<sub>10</sub> mass concentrations with  $r = 0.39$  for  $n = 2666$ ). The weak correlation ( $r = 0.26$ ,  $n = 2946$ ) between NR-PM<sub>1</sub> and PM<sub>1</sub> might be explained by the contribution of refractory  
20 material (DD and SS) to the total PM<sub>1</sub>, while the absence of correlation ( $r = 0.08$ ,  $n = 3424$ ) between NR-PM<sub>1</sub> and PM<sub>10</sub> was expected, as well as the low average contribution (8%) of NR-PM<sub>1</sub> to PM<sub>10</sub>. Indeed, the coarse fraction of aerosol (PM<sub>10</sub>) at this site is dominated by DD and SS (Flament et al., 2011). NR species represent on average 71% of the total PM<sub>1</sub>, which underlines the significant influence of refractory material in the fine fraction of aerosol measured at M'Bour. During IOP-1, as shown in Figure 3b, despite an important variability (values ranging between  
25 4 and 25%) submicron particles (both refractory and non-refractory fractions) represent on average 11% of the PM<sub>10</sub> fraction whatever the day type. This pattern has already been observed at other sites influenced by Saharan emissions, and consequently under the influence of DD like Granada (Titos et al., 2015) or Cape Verde (Pio et al., 2014).

Despite similar orders of magnitude between the values of NR-PM<sub>1</sub> and total PM<sub>1</sub>, their ratio exhibits different trends  
30 depending on day type (Figure 3c). When comparing PM<sub>1</sub> and NR-PM<sub>1</sub> concentrations for marine days, NR species appeared to account for most of the PM<sub>1</sub> fraction over IOP-1 (slope: 0.71,  $r = 0.82$ ,  $n = 452$ ), suggesting a minor influence of sea salt in the PM<sub>1</sub> fraction. This conclusion is consistent with the analysis of Flament et al. (2011) during the AMMA SOP-0 in M'Bour, with a reported PM<sub>2</sub> fraction composed of 18 to 77% of DD and less than 20% of soluble ions (dominated by NaCl). Additionally for continental and sea breeze scatter plots also reported in Figure  
35 3c, the discrepancies between NR- and total PM<sub>1</sub> mass concentrations are higher (slopes of 0.49 and 0.56,

respectively), underlying that continental air masses – predominant during those days – carried additional refractory material such as DD in the submicron fraction. The unaccounted fraction was determined as the difference between the gravimetrically measured  $PM_{10}$  mass concentration and the sum of chemical species from ACSM (Org,  $NO_3$ ,  $SO_4$ ,  $NH_4$ , Chl) and aethalometer (BC, Fe) measurements. It corresponded to 27%, 26% and 16% of the  $PM_{10}$  mass for continental, sea breeze and marine days, respectively (see Figure S3). A more significant difference could have been expected for continental compared to other days, but this might be explained by the absence of  $PM_{10}$  mass measurements during the more intense dust events, as mentioned previously. Nevertheless, these results stress the need to apply Fialho et al. (2014) deconvolution in order to separate DD and BC absorption contribution.

### 3.1.2 Estimation of absorbing compound concentrations in $PM_{10}$

Fe and BC concentrations obtained after correction led to averaged values of  $(0.55 \pm 0.85)$  and  $(0.36 \pm 0.37) \mu g m^{-3}$ , respectively, over the whole IOP-1 dataset. The deconvolution led to an average decrease of 45% of BC concentrations (factor of 2.2), which is much higher than the 11% decrease observed by Doumbia et al. (2012) in Dakar where local BC sources are predominant. In our study the decrease even reached 83% under the influence of Saharan dust events and therefore the influence of DD on absorption measurements could never be neglected. As depicted in Figure 4, BC concentrations hardly exceeded  $3 \mu g m^{-3}$ , except throughout punctual and short-term episodes during which they reached higher values, with a half-hourly average maximum of  $3.6 \mu g m^{-3}$  reached on April 2, 2015. The higher concentrations can be attributed to local anthropogenic combustion processes as BC concentrations present a significant correlation ( $r = 0.79$ ) with the ACSM m/z 57 tracer of all types of combustion.. BC concentrations measured in M'Bour are on average much lower than those measured in Dakar during POLCA (Doumbia et al., 2012), where BC yearly average was  $(10.5 \pm 3.5) \mu g m^{-3}$ . The lower concentrations measured here can be explained by the differences in sampling site type and population with the IRD center being located at the outskirts of the city of M'Bour (180 000-200 000 inhabitants) area while the site in Dakar (about 3 million inhabitants within the metropolitan area) was located in an urban area. It can be noted that the range of BC concentrations ( $0.01$ - $3.6 \mu g m^{-3}$ ) obtained during IOP-1 in M'Bour is within the same order of magnitude than the one reported by Lioussé et al. (2010) for the rural site of Djougou, Benin between Dec. 2005-Feb. 2006 ( $0.4$ - $8.2 \mu g m^{-3}$ ).

Fe concentrations estimated from  $PM_{10}$  absorption measurements are considered as an indicator of DD in the fine fraction. The following comparisons were carried out only on coincident measurements, due to missing data in the  $PM_{10}$  and  $PM_{10}$  datasets, corresponding to lower average concentrations of Fe ( $0.39$  and  $0.53 \mu g m^{-3}$  for the  $PM_{10}$  and  $PM_{10}$  data comparison, respectively). Although weak correlations were found between Fe and total  $PM_{10}$  concentrations ( $r = 0.55$ ) and unaccounted  $PM_{10}$  ( $r = 0.47$ ), Fe concentrations showed higher correlations with  $PM_{10}$  ( $r = 0.70$ , see Figure 4). This could be explained by the lack of  $PM_{10}$  mass concentration measurements during intense dust events, as well as DD domination in the coarse fraction, while the fine fraction is mainly driven by NR and BC species during most of the IOP-1 (Figure 3c). As depicted in Figure 4, most of the low iron concentrations were related to days under marine influence, while the highest Fe concentrations ( $> 8.0 \mu g m^{-3}$ ) are generally associated

with continental and sea breeze days. These maxima also coincide with  $PM_{10}$  highest concentrations ( $> 400 \mu g m^{-3}$ ) and confirm iron as a constituent of mineral dust emitted by the Saharan and Sahel regions.

From the only study in the literature focusing on iron concentrations in the submicron fraction in West Africa (Val et al., 2013), we could infer an elemental iron contribution of 7.8% to  $PM_1$  dust, in Dakar, in the absence of dust events.

5 Other studies focused on dust gave the iron contribution for size fractions higher than  $PM_1$ , thus no straightforward comparisons can be made with our average ratios of  $Fe/DD_{PM_1}$  (20, 23, 21 and 16% for respectively IOP-1, continental, sea breeze and marine days). It can nevertheless be interesting to have in mind values retrieved within the same region as it is known that iron oxides mainly belong to the finest fraction (Journet et al., 2014; Kandler et al., 2009) and therefore the elemental iron contribution should be lower for larger sizes, which is consistent with  
10 values reported in Table S2.2.

### 3.1.3 $PM_1$ average chemical composition

Table 1 reports ACSM measurements performed at M'Bour between March 20 and June 22, 2015, as well as other field campaigns carried out worldwide. This study shows an average value of  $5.4 \mu g m^{-3}$  for NR- $PM_1$  with a maximum half-hourly average of  $68.3 \mu g m^{-3}$ . The total  $PM_1$  mean concentration (including BC and Fe) is  $8.2 \mu g m^{-3}$   
15 (maximum half-hourly average:  $143 \mu g m^{-3}$ ), a value which is about 10 times lower than the  $PM_{10}$  mean concentration of  $103.5 \mu g m^{-3}$  over the same period. This  $PM_{10}$  average is consistent with the range of monthly averages reported by Kaly et al. (2015) at M'Bour for the March-June period of 2006-2010 (between 63 and  $126 \mu g m^{-3}$ ). When compared to similar studies conducted around the world, M'Bour clearly appears much less polluted than megacities like Beijing (Sun et al., 2012) or Paris area during winter (Petit et al., 2014). The mean NR- $PM_1$   
20 measured at M'Bour is close to the only other value reported in Africa for Welgegund, South Africa (Tiitta et al., 2014), continental background sites such as MontSec, Spain (Ripoll et al., 2015) or during summer in Paris with an average of  $4.5 \mu g m^{-3}$  (Petit et al., 2015).

The average NR- $PM_1$  chemical composition measured in M'Bour was composed of OM (39%),  $SO_4$  (35%),  $NH_4$  (15%)  $NO_3$  (9%) and Chl ( $\sim 1\%$ ), which is again rather similar to what was observed in South Africa by (Tiitta et al.,  
25 2014). Indeed, the OM and  $SO_4$  predominance has been also observed in the majority of cities where ACSM (see Table 1) and AMS (Zhang et al., 2007) campaigns were implemented. Nonetheless, during winter, some European sites like Paris (Petit et al., 2015), Cabauw (Schlag et al., 2015) or Zurich (Lanz et al., 2010) present a fine fraction mainly dominated by nitrate and organic species. In our case these differences could be explained both by the semi-volatile nature of  $NH_4NO_3$  combined with the limited use of fertilizers that prevent  $NH_3$  emissions and ammonium  
30 nitrate formation, and more sources of non sea salt(nss)- $SO_4$  such as marine DMS oxidation processes. The first point can be assessed by emission inventories that provide annual  $NH_3$  emissions (in 2010) of 53 kT in Senegal against 870 kT in France and 204 kT in the Netherlands (source EC-JRC/PBL. EDGAR version 4.2. <http://edgar.jrc.ec.europa.eu/>, 2011). nss- $SO_4$  comes from secondary origin and has been investigated in  $PM_{10}$  at the Cape Verde Atmospheric Observatory (Fomba et al., 2014). This study showed increased concentrations of nss- $SO_4$   
35 during dust events, linked to the oxidation of anthropogenic  $SO_2$  transported by continental air masses. They also evidenced a seasonal variability of nss- $SO_4$  for marine air masses, increasing during summer, which was attributed to

increased photochemistry and changes in the emission of dimethyl sulfide (DMS) due to higher biological activities in the ocean. This activity can be traced back using satellite data from AQUA/MODIS, in particular the algae concentrations along the Senegalese coast (Ocean biology processing group, 2003).

Figure 5 represents the average contributions of NR-PM<sub>1</sub> species, BC and Fe in PM<sub>1</sub> over the entire IOP-1 and more specifically for continental, sea breeze and marine days. Total PM<sub>1</sub> pie charts, including unaccounted-for aerosol species obtained by chemical mass closure, have been reported in the supplementary material section (Figure S3). Figure 5 shows that although an almost equal proportion of organic and sulfate species (31 and 32% respectively) was measured on average over the whole IOP-1, strong differences regarding day types can be highlighted: continental and sea breeze days present similar averaged compositions, with a major contribution of OM (36-40%) followed by SO<sub>4</sub> with 21-24%. Similarities between the two profiles are probably due to a longer influence of northern wind compared to western ones during sea breeze days. On the other hand, for marine days the dominant fraction is sulfate (40%) while OM averaged contribution decreased to 25%. These changes could be explained by (i) oceanic air masses known to carry higher amount of sulfate species from the oxidation of dimethylsulfide (DMS) and organosulfur gases (Charlson et al., 1987; Fitzgerald, 1991) and (ii) long-range transport of polluted air masses from the continent, carried back to M'Bour through oceanic air masses. BC and Fe from anthropogenic and continental origins, respectively, are also less abundant during marine days compared to continental/sea breeze days with fractions decreasing from 7 to 3% and 14-16% to 3%, respectively.

Comparable dynamics was already observed at M'Bour during AMMA SOP-0. For instance, Haywood et al. (2008) highlighted that BB aerosols carried in altitude (~3 km) from the African continent to the Atlantic Ocean were then driven back through south-westerly winds. Similar contributions have been observed in Welgegend (Tiitta et al., 2014) where PM<sub>1</sub> measured during the dry season were dominated by OM (57%), followed by SO<sub>4</sub> (16%) and BC (10%), and the wet season marked by high contributions of SO<sub>4</sub> (42%) and lower contributions of OM and BC (35 and 4%, respectively). In M'Bour, we obtained a significant correlation ( $r = 0.74$ , Figure S9) between the OM and BC time series and an average BC/OM ratio of 0.15, whatever the day type, suggesting similar emission sources and therefore pointing to continental origins either directly linked to combustion processes, as both species displayed a more important contribution during continental and sea breeze days, or due to the mixing of anthropogenic emissions with biogenic precursors or secondary organic aerosols (SOA).

Aerosol acidity can be considered as an indicator of the age of particles as they will get neutralized during their stay in the atmosphere. In order to estimate the degree of neutralization of ACSM inorganic species, NH<sub>4</sub> measured concentrations (as NH<sub>2</sub><sup>+</sup>, NH<sub>3</sub><sup>+</sup> and NH<sub>4</sub><sup>+</sup> ions) are compared to predicted ones, which are equal to the amount of NH<sub>4</sub> required to fully neutralize sulfate, nitrate and chloride anions according to the following equation (Zhang et al., 2007):

$$NH_{4,pred} = M(NH_4) \times \left( 2 \times \frac{SO_4^{2-}}{M(SO_4^{2-})} + \frac{NO_3^-}{M(NO_3^-)} + \frac{Cl^-}{M(Cl^-)} \right) \quad (11)$$

with SO<sub>4</sub><sup>2-</sup>, NO<sub>3</sub><sup>-</sup> and Cl<sup>-</sup> the mass concentrations of inorganic species in μg m<sup>-3</sup> and M(X) their molecular weights (NH<sub>4</sub> 18; SO<sub>4</sub> 96; NO<sub>3</sub> 62; and Cl 35.5 g mol<sup>-1</sup>).

The slope obtained between NH<sub>4</sub> measured and predicted (1.02,  $r = 0.92$ ; see Figure S3a) underlined that most of inorganic species are neutralized over IOP-1, and additionally that there is no strong bias in the calibration values

used for ACSM measurements. Nonetheless, a few points digress from the 1:1 line indicating partially neutralized species (as mentioned above). On one hand, points significantly above the 1:1 ratio suggest the presence of  $\text{NH}_4$  under other forms than  $(\text{NH}_4)_2\text{SO}_4$ ,  $\text{NH}_4\text{NO}_3$  and  $\text{NH}_4\text{Cl}$ . As these points also correspond to higher levels of OM, BC and chloride, circled in red (Figure S4c), they might be related to nitrogen-containing species associated with combustion processes at low RH ( $<50\%$ ; Figure S3a-b), where chlorine could come from the combustion of sea salt and/or chlorine-containing materials such as plastics. On the other hand, 23% of the data are associated to a  $\text{NH}_{4,\text{meas}}/\text{NH}_{4,\text{predict}}$  ratio inferior to 0.75 and correspond to points under the 1:1 line in Figure S3a. For such points, the amount of  $\text{NH}_4$  predicted is overestimated in comparison to the amount measured on site, and considering that  $\text{NH}_4$  will preferentially react with  $\text{SO}_4$ , other anions like  $\text{NO}_3$  and Cl are partially under chemical states other than ammonium nitrate and chloride. As mentioned previously and developed in section 3.2, this can be explained by chloride species emitted by local combustion processes but also by  $\text{HNO}_3$  adsorption on dust as already reported in the literature (Fairlie et al., 2010; Savoie et al., 1989) and this is consistent with ratio values inferior to 0.75 which are mainly observed while the site is under dust influence (Figure S3b). Nevertheless these periods also correspond to low levels of inorganic species in  $\text{PM}_{10}$ .

### 3.1.4 Variations of $\text{PM}_{10}$ chemical species

Figure 6 displays the 30-minute temporal variability of NR- $\text{PM}_{10}$  species during IOP-1. At such a timestamp a total of 13 pollution events – characterized by NR- $\text{PM}_{10}$  concentrations exceeding a threshold value of  $15 \mu\text{g m}^{-3}$ , corresponding to three times the average – were detected. In terms of chemical composition, the highest average - over the whole IOP-1- concentrations were obtained for OM and  $\text{SO}_4$  with respective values of 2.12 and  $1.85 \mu\text{g m}^{-3}$  ( $n = 3931$ ). Moreover OM concentrations could present a high variability over short periods, like on May 12, 2015 when OM jumped from 0.9 to  $61.7 \mu\text{g m}^{-3}$  over an interval of 30 minutes, while the sum of other NR- $\text{PM}_{10}$  species remained below  $10 \mu\text{g m}^{-3}$ .

OM and  $\text{SO}_4$  daily fractions exhibit opposite trends, with periods dominated by OM ( $> 30\%$ ) at the beginning of IOP-1 and from May 20 to June 8, 2015, corresponding to days under continental or sea breeze influences. OM concentrations encountered during these periods are generally related to punctual intense episodes, suggesting an influence linked to emissions by rather local anthropogenic activities rather than long-range transport sources. Periods from April 25 to May 21 and after June 9, 2015, associated with oceanic air masses, are dominated by  $\text{SO}_4$  ( $> 30\%$ ), with generally more moderate concentrations and less intense peaks, except for May 13<sup>th</sup> 2015, with NR- $\text{PM}_{10}$  reaching its maximum at  $68 \mu\text{g m}^{-3}$ .

The daily profiles of all identified  $\text{PM}_{10}$  species and meteorological parameters (wind speed, temperature and wind roses) are presented in Figure 7 according to day types. Strong similarities can be observed between the continental and sea breeze daily profiles (Fig. 7a-b), both presenting a morning peak around 8 am marked by a distinct rise in OM ( $> 4 \mu\text{g m}^{-3}$ ) and BC ( $\sim 1 \mu\text{g m}^{-3}$ ) concentrations and to a lesser extent in  $\text{NH}_4$  and chloride concentrations. Continental and sea breeze daily profiles also show a common peak at 8 pm, less intense than the morning one, but characterized by an increase in OM and BC. It can be noticed that this evening peak is less pronounced for continental days (OM  $\sim 3.5 \mu\text{g m}^{-3}$  and BC  $\sim 0.7 \mu\text{g m}^{-3}$ ) than for sea breeze days (OM  $\sim 4.5 \mu\text{g m}^{-3}$  and BC  $\sim 0.9 \mu\text{g m}^{-3}$ ).

$\text{m}^{-3}$ ). As mentioned previously, the BC/OM ratio is on average of 0.13-0.14 for sea breeze and continental days (see Figure S9) but during the morning and evening peaks these ratios can reach a maximum of  $\sim 0.25$  meaning that BC emissions are enhanced during these hours. A specific pattern of continental days is a peak measured at noon for OM and BC concentrations (constant BC/OM ratio  $\sim 0.16$ ), probably combining local emissions and reduced dispersion due to dynamic phenomena as suggested by the slight wind speed decrease. On the other hand, for sea breeze days a peak occurring at 3 pm, with an intense increase in OM, a moderate one in  $\text{SO}_4$  and almost no variation of BC (ratio of 0.1), coincide with the sea breeze establishment (discernible through wind plots and the slight drop in temperature). BC for continental and sea breeze daily profiles show a maximum intensity of  $1.1 \mu\text{g m}^{-3}$  for the continental morning peak (8 am), a value which is quite consistent with maximal hourly concentrations (up to  $4 \mu\text{g m}^{-3}$ ) measured at 8 am, 4 pm and 8 pm in M'Bour by Deboudt et al. (2010). These peaks are measured for air masses coming from the continent and correspond to traffic and/or cooking hours. Chloride peaks associated to intense OM and BC ones tend to confirm combustion sources for these species, as previously observed during winter in Beijing by Sun et al. (2013).

The marine averaged daily profiles show a very distinctive pattern, compared to continental/sea breeze days (Fig. 7a), and are characterized by a sharp decrease of OM, BC and Fe, with nitrate, ammonium and chloride presenting rather constant profiles, while sulfate exhibits a higher and almost constant concentration of  $2.4 \mu\text{g m}^{-3}$ . This pattern as well as the sulfate peak associated with the sea breeze tends to confirm the regional transport of sulfate to M'Bour through oceanic air masses. It is noticeable that for marine days, OM and BC profiles reached maximum concentrations of  $2.5$  and  $0.35 \mu\text{g m}^{-3}$  during the night (between 8 pm and 2 am), in coincidence with low wind speed (Fig. 7d). Thus, this night time increase of concentrations measured for marine days might be due to lower dilution of aerosols species from local emissions. The results obtained at M'Bour for marine days are in agreement with those reported by Topping et al. (2004) in Korea, with inorganic species such as  $\text{SO}_4$ ,  $\text{NO}_3$  and  $\text{NH}_4$  increasing significantly during days under marine influence.

In Figure 7b, Fe and BC profiles showed distinctive behaviors depending on day types. As expected, both profiles for marine days are characterized by very low concentrations of both BC and Fe in comparison to those measured for sea breeze and continental days. In the latter cases, a major difference can be observed for Fe concentrations which are almost twice higher than BC ones. Fe exhibits an additional intense peak around 3 pm and concentrations above  $1.5 \mu\text{g m}^{-3}$  from noon to 8 pm during continental days, which can be attributed to the intense dust events occurring around the end of March and on April 10<sup>th</sup> when comparing average and median profiles. These patterns suggest a transport of BC and DD (through Fe) by continental air masses – from the areas north and north-east of M'Bour. Most probably air masses loaded in DD coming from the Saharan region (Fe continental profile) are then enriched in BC during their transport above cities. Nonetheless local traffic activities may also be a non-negligible source of dust through resuspension processes, which would also explain the synchronized peaks of BC and Fe observed for continental profiles even when excluding desert dust events.

## 3.2 Origins and sources of aerosols

### 3.2.1 Geographical origins of chemical species

As observed previously, most of the winds reaching M'Bour during IOP-1 were associated with the north and west sectors, carrying respectively air masses from the continent and the ocean, with an averaged wind speed of  $2.6 \text{ m s}^{-1}$ .

5 These results are consistent with the five-year measurements of wind direction reported by Kaly et al. (2015) in M'Bour for the dry season. From back-trajectory analysis (Figure S5a) three different clusters were encountered during the whole period. The prevailing one (77% for the whole IOP-1; 91, 80 and 43% for continental, sea breeze and marine days, respectively) evidences air masses transported along the Western African coast and over Dakar. A second cluster corresponds to air masses purely originating from the ocean (19% of the total back-trajectories) and  
10 appeared as two clusters during marine days. A last cluster coming from the Saharan desert contributes only 4% of the IOP-1 air masses but reaches 9 and 10% for the continental and sea breeze days, respectively. Figure 8 presents pollution roses obtained combining the time series of the different  $\text{PM}_{10}$  components and co-located surface wind direction/speed measurements, thus offering a first insight into the geographical origins of chemical species. NWR plots and PSCF maps can be found in Figure S5b and S5c, respectively. Similar spatial origins can be observed for  
15 several species; in particular, OM, BC and Chl maximum concentrations are rather associated with north-east (NE) winds during morning peaks and north-west (NW) winds at the end of the day (Fig. 7), pointing out to a common origin of the higher concentrations observed for these species, that would be linked to combustion processes due to the presence of BC. BC and  $\text{NO}_3$  both exhibit local and regional influences, as suggested by their NWR plots (Figure S5b). The corresponding PSCF maps (Figure S5c) indicate regional background concentrations could come from  
20 anthropogenic emissions from Dakar (~1 million inhab. within city limits and ~3 in the metropolitan area) and possibly from maritime traffic along the Western African coast.

Figure 8 also highlights an oceanic origin for some OM (with moderate intensity),  $\text{SO}_4$  (as already observed in Fig. 5),  $\text{NO}_3$  and  $\text{NH}_4$ . There is no clear trend linked to the wind speed (slower along the coast and higher when perpendicular to it), meaning particulate chemical species are rather transported or formed above the ocean than  
25 directly emitted by sea spray (Ovadnevaite et al., 2012). Emissions of DMS and organosulfur gases by microorganisms (as mentioned previously) could explain part of the  $\text{SO}_4$  and OM concentrations observed when the site is under western influence. These species may also be released by anthropogenic activities in distant cities like Dakar, whose emissions may be carried toward the ocean and brought back to M'Bour by western winds. This hypothesis is also supported by back-trajectory analysis (Figure S5a). A long-term  $\text{PM}_{10}$  chemical characterization  
30 conducted in Cape Verde by Fomba et al. (2014) has also shown that marine air masses were mostly composed of sulfate (10% on average) rather than organic matter (3.5%) but the proportion in  $\text{PM}_{10}$  is more balanced.

Regarding the iron pollution rose and NWR plots reported in Figure 8 and Figure S5b, maxima are measured when the site is under the influence of NE winds. The NWR plot evidences both local emissions possibly linked to traffic resuspension of DD and a regional component, that the Fe PSCF map clearly attributes to the Saharan region. For  
35 such directions we also observe maximum values of the total  $\text{PM}_{10}$  concentrations ( $> 60 \mu\text{g m}^{-3}$ ), which correspond to the April 10, 2015, most probably a resuspension event following previous dust storms, as observed on  $\text{PM}_{10}$  and Fe concentrations time series (reported respectively on Figure 3 and 4).



### 3.2.2 Source apportionment of OM

PMF was first applied without constraints on the whole IOP-1 organic database and then separately on continental, sea breeze and marine extracted datasets (see also Supplementary Information Appendix S4). Three to ten factors were tested and for each run, only solutions with a normalized  $Q/Q_{\text{exp}}$  ratio close or inferior to 1 were taken into account. Mass spectra were compared to reference profiles for identification and the consistency with daily profiles was checked. Without any constraints applied to the model, one or two factors identified as oxygenated organic aerosols (OOA, dominated by the  $\text{CO}_2^+$  fragment at  $m/z$  44) were easily retrieved for all datasets. An unknown factor with peaks at  $m/z$  58, 60, 83 and 91 appears for the whole IOP-1 when the number of factors increases (and is mixed with one of the OOA in the reduced datasets). This factor appeared constantly above 4 factors in the unconstrained runs from 3 to 10 factors (Appendix S6, Figure S6.1) and was associated with one of the OOA for the continental, sea breeze and marine 4-factor unconstrained solutions (Figure S6.2). Besides, the model encountered difficulties to separate hydrocarbon-like (HOA) from cooking-like (COA) organic aerosol for the entire IOP-1 dataset and the continental and marine days. Both COA and HOA share similar  $m/z$  peaks at 27, 41, 55 ( $\text{C}_n\text{H}_{2n-1}^+$ ) and 29, 43, 57 ( $\text{C}_n\text{H}_{2n+1}^+$ ) that correspond to hydrocarbon fragmentation. Nonetheless, they can be differentiated based on 41/43 and 55/57 ratios, more important for COA (Fröhlich et al., 2015a; Mohr et al., 2012), while HOA presents more specific and intense peaks at 69-71. Moreover under continental influence, they tend to be emitted from the same wind directions corresponding to the urbanized area from NW to NE. A good separation with characteristic factor profiles was nonetheless obtained for sea breeze days which present a more variable dynamics, with 4 factors identified, namely HOA, COA, as well as more oxidized and less-oxidized OOA (mixed with the unknown factor) (Appendix S6, Figure S6.2c). The unknown factor presents a rose plot and a daily profile consistent with local emissions from the open waste burning areas of Gandigal (NW) and Saly Douté (NE) and a fish-smoking area also located in the NE of M'Bour (Figure 1 and Appendix S6, Figure S6.3), hence it has been designated as LCOA (Local Combustion Organic Aerosol). Since the behavior of Chl had also been suspected to come from the same sources, PMF solutions adding the  $m/z$  36 signal in the input matrix were investigated, and a solution is presented in Appendix S8, where regional OOA accounts for  $\sim 3/4$  of the OOA and local OOA  $\sim 1/4$ . No biomass burning OA (BBOA) profile appeared neither in our unconstrained (up to 10 factors) runs, nor when HOA and COA were themselves constrained. Furthermore, local practices tend to use dry leaves and branches to feed livestock rather than as combustion fuel, and cooking in the urban area is mainly done on gas stoves. IOP-1 occurring at the transition between dry to wet seasons, the possibility of long-range emissions of BB from Savannah fire, like the one observed for example in South Africa (Tiitta et al., 2014) and northern Australia (Milic et al., 2016), or even other BB regional sources, was not discarded at first. Therefore, an average BBOA profile (Ng et al., 2011b) was used to constrain the PMF solution with different  $a$ -values. Using a rather strong constraint of  $a = 0.3$  led to a satisfactory BBOA profile but either stable solutions presenting a mixture between LCOA and part of the OOA factor but no COA, or when LCOA, OOA and COA were well separated, the BBOA profile presented missing fragments and a high run-to-run instability. Moreover, solutions for more moderate constraints ( $a \geq 0.5$ ) led to a BBOA profile with unusually low or missing important fragments (such as  $m/z$  60) and an increasing correlation with COA (Crippa et al, 2013). Besides, the important photochemistry observed on site coupled with levoglucosan ( $m/z$  60, 73) fast reactivity under photo-oxidative conditions (Hennigan

et al., 2010) might lead to a fast transformation of BBOA into SOA (which would appear as an OOA factor in our PMF solution). Finally, additional in situ or remote sensing optical instruments specifically implemented for the SHADOW campaign, such as ground-based and airborne sunphotometers or the LILAS multiwavelength Mie-Raman lidar (Veselovskii et al., 2016), did not detect the presence of BB aerosol influence. For all these reasons, we decided not to constrain BBOA in our final solutions. In order to refine the solution, and due to the possible specificity of local emissions, the PMF model was run with mild constraints on the primary factor profiles observed in the different unconstrained runs (see Fig. S6.2) that is to say COA (Crippa et al., 2013) and HOA (Ng et al., 2011b) using the  $\alpha$ -value approach with 30 to 90% of freedom ( $0.3 < \alpha < 0.9$ ) as explained in Canonaco et al. (2013). Indeed HOA are generally emitted by diesel or fuel exhaust, although in rural cities they have also been related to cooking activities (Sun et al., 2012). It has also been reported that African fuels supplied directly by Western company-owned petrol stations present higher levels of sulfur and polyaromatics, and that others are generally a mixture of refinery intermediate products and other (mostly unknown) chemicals, which could hamper the finding of a satisfactory solution. The robustness of the optimal solution was checked by 50 random seed iterations.

A final constrained solution of 4 factors is presented in Figure 9 through their respective mass spectra with associated pollution rose plots and daily profiles for continental, sea breeze and marine days. The three primary (POA) factors linked to anthropogenic activities, that is to say HOA, COA, and LCOA corresponded to 18, 30 and 3% of the organic fraction, respectively. HOA and COA contributions to the OA fraction tend to be more important for continental and sea breeze days with respectively 21-24% and 24-31% than for marine days (11-20%), while LCOA slightly increases from 2 to 7%. The HOA profile is well correlated with BC ( $r = 0.79$ ) and  $m/z$  57 ( $r = 0.98$ ). No specific external tracers have been identified nonetheless COA temporal variability appeared to correlate well with BC ( $r = 0.73$ ). The HOA rose plot shows marked peaks in the directions of the two open waste burning areas and of the fish-smoking area located northeast of the site in the outskirts of M'Bour. HOA and Chl NWR plots are very similar, which suggests either common sources or a mixture of both compounds in the air masses which resulted into a correlation of 0.64 between these two variables. COA main origin in the northwest corresponds to the touristic area of Saly where a number of restaurants are located. BC concentrations previously linked to OM species present close correlations with both HOA and COA but this might be explained by the correlation of 0.82 between both time series suggesting concomitant emissions between traffic and cooking sources. The variability depicted by their continental and sea breeze daily profiles (Fig. 9b) highlights anthropogenic emissions of COA and HOA with pronounced peaks during morning and evening ( $0.46$  to  $0.55 \mu\text{g m}^{-3}$ ) corresponding to human activities. The COA and HOA profiles present an additional peak after 11 am, reaching a maximum around noon then decreasing after 2 pm for continental days. The COA, OOA – and to a much lower extent, the HOA – sea breeze profiles differed from the continental ones by a delay in the midday peak which rises only after 2 pm. This difference could be explained by anthropogenic aerosols emitted in the morning, then transported toward the ocean, and carried back on site through sea breeze phenomena. A similar pattern could have been expected from HOA, but the low concentrations observed suggest faster oxidation processes occurring over the ocean which would contribute to the higher OOA peak. Both COA and HOA factors present low background concentrations during marine days.

As for LCOA which is a very small fraction of the total OA, the fact that it nonetheless consistently appears in the PMF analysis under both unconstrained and constrained conditions, suggests a specific behavior uncorrelated with other sources. Its robustness has been tested under various starting conditions (50 seed iterations) and through rotational ambiguity exploration (F-peak tested between -5 and +5 with a step of 0.5). Despite the fact that Chl species were presenting similar wind sectors origins, its correlation with LCOA remains low ( $r = 0.44$ ) while LCOA presents higher correlation with  $m/z$  36 and 58 ( $r = 0.55$  and  $0.84$ , respectively). This is mainly due to the influence of refractory chloride (NaCl) in our Chl measurements; which has been observed through  $m/z$  35 negative values likely resulting from a slow vaporization both during filter and non-filter measurements (Nuaaman et al., 2015). Nonetheless  $m/z$  36 ( $\text{HCl}^+$ ) was mostly positive ( $0.03 \pm 0.03$ , see Figure S7) confirming that non-sea salt chloride was also detected. Indeed, if sea salt was predominant in LCOA, NaCl could explain the  $m/z$  58 and 60 signals, but one would have expected a maximum on marine days, whereas LCOA pollution rose and NWR plots clearly point out toward the local combustion areas already mentioned previously, and also identified in the chloride rose plot (Figure 8). Although coal combustion used for cooking has been identified as a potential source of chloride emissions (Ianniello et al., 2011; McCulloch et al., 1999), this practice has not been observed in the area. However, chloride species may be emitted from household waste burning/smoldering, for which particle-bound polychlorinated dibenzo-p-dioxins and dibenzofurans (PCDD/Fs) and polychlorinated biphenyls (PCBs) have been measured in previous studies (Gullett et al., 2001; Lemieux et al., 2004; Tue et al., 2016; Zhang et al., 2009); or from sea salt particles subject to high-temperature combustion processes (since this factor is also observed to a lesser extent in the direction of the fish-smoking area). Besides the NWR plots of Chl (local influence) and LCOA (both local and regional) rather suggest the presence of chlorinated organics. The PSCF maps identify two possible origins, one clearly from the ocean that could be related to chlorine-driven photo-oxidation processes (Hossaini et al., 2016) and the other linked to air masses carried over Dakar where similar massive anthropogenic emissions from waste burning could be expected from Mbeubeuss, the largest dumpsite in Senegal located 25 km north-east of Dakar along the coast, which receives 250,000 tons of garbage per year from the Dakar region (Cissé, 2012).

Additionally, the measured  $\text{NH}_4$  was higher than the predicted one in the directions of the waste burning areas - especially from the North-East (Figure S4b), also suggesting the formation of nitrogen-containing compounds that could lead to  $\text{R-N}^+$  or  $\text{R-NO}^+$  fragments at these same masses although high-resolution measurements would be needed to confirm this hypothesis. LCOA also present its most intense peaks in the morning ( $0.04 \mu\text{g m}^{-3}$ ) and some more moderate in the evening ( $< 0.03 \mu\text{g m}^{-3}$ ) for continental and sea breeze daily profiles, characteristics of point sources and/or local emissions. These may be linked to the start of the fires in the morning for the open waste burning areas and an evening increase of the OM due to temperature drop that would shift the partitioning of semi-volatile species toward the particulate phase. On the contrary its marine profile shows constant but higher concentrations all day long ( $\sim 0.03 \mu\text{g m}^{-3}$ ) with an increase after 8 am, which explains the slightly higher contribution to the OA fraction for the latter.

OOA are often considered as secondary organic aerosols (SOA) formed through gas-conversion processes of Volatile Organic Compounds (VOCs) or photochemical oxidation of primary OA emitted by biogenic (such as plants or algae) and/or anthropogenic sources. The hot temperatures and intense solar irradiation encountered in the region

enhance these processes and can explain the major contribution (45%) observed for the OOA factor during IOP-1, and the predominance (~3/4) of the more-oxidized fraction in the solution presented in Appendix S8. Its profile showed intense peaks at  $m/z$  18 and 44 ( $f_{44} = 0.36$ ) and low 43/44 ratios (0.04), which underlined the high level of oxidation characteristic of aged particles, and presented a correlation of 0.88 with the OOA averaged profile reported by Ng et al. (2011). In our study, the temporal variability of OOA shows a higher correlation with  $\text{NO}_3$  than  $\text{SO}_4$  ( $r = 0.56$  against  $r = 0.24$ ). As  $\text{NO}_3$  species are generally semi-volatile and associated with less aged air masses (Mohr et al., 2012), OOA might not be only emitted by long distant sources, as also suggested by its NWR plot (Figure S5b). This is highlighted by daily continental and sea breeze profiles rising around 8 am, noon and 8 pm which emphasize direct emission of oxidized organic aerosols from anthropogenic activities. Also, it has been mentioned previously that  $\text{NO}_3$  might not be locally emitted (Figure 8 and S5b) and OOA highest concentrations being associated with wind speeds above  $3 \text{ m s}^{-1}$ , we attribute also a regional origin to this factor. Both the OOA correlation with  $\text{NO}_3$  and the fact that its daily cycles progressively increase/decrease with sunrise/sunset suggest an important and fast photochemistry (Robinson et al., 2007). The OOA rose plot shows rather similar concentrations regardless of wind sectors, even if some concentrations superior to  $1.5 \mu\text{g m}^{-3}$  are connected to western wind influences (Figure 9). This oceanic origin is also highlighted by OOA sea breeze profile, which shows a maximum of  $0.7 \mu\text{g m}^{-3}$  reached around 3 pm (Figure 9). It indicates that this SOA formation is enhanced during OA transport over the ocean which under specific atmospheric conditions can be initiated by chlorine atoms (Hallquist et al., 2009). The OOA PSCF map (Figure S5c) seems to trace back its origin along the entire Western African coast, where shipping emissions could be a major source of organic aerosols. OOA increasing during daytime regardless of day type, their high oxidation level and important contribution to OA, especially during marine days (62%), support emissions by regional sources. As shown by the PSCF map (Figure S5c), higher OOA concentrations are associated to air masses that moved along the coast and could transport oxidized anthropogenic species to the receptor site.

Previous observations of OM from daily filter measurements in the  $\text{PM}_{2.5}$  fraction during AMMA SOP-0 were associated maximum values with winds coming from the coast (NW) and the ocean (W) (Flament et al., 2011) and attributed to emissions by local sources and cities along the Senegalese coast, suggesting they could originate from wood burning, cooking and dry leaf/grass burning. Only considering biomass burning and fossil fuel combustion as contributing to the absorption measurements during their field campaign in Dakar, Doumbia et al. (2012) also reported 12% of biomass burning emitted by regional sources against 88% by fossil fuel. Our measurements over a period of three months at high-time resolution suggest, as mentioned before, that biomass burning from local sources is rather negligible in the M'Bour area during the transition period from dry to wet seasons. Cooking, traffic and other local combustion sources such as traditional fish smoking and household waste burning have been identified as the primary local anthropogenic sources of OM.

#### 4 Conclusions

The deployment of high time resolution instruments at the West African coastal site of M'Bour (Senegal) during three months encompassing the end of the dry season and the transition period toward the wet season of 2015 allowed to investigate the temporal variability and chemical composition of the poorly characterized  $\text{PM}_{10}$  aerosols in

this region. The average NR-PM<sub>1</sub> concentration (5.4 µg m<sup>-3</sup>) was relatively low, comparable to levels generally reported in rural environments and also close to the one observed at a South African site. Although marine influence was dominant, various dynamic conditions were encountered during the campaign, with intense dust events, sea breeze phenomena and several anthropogenic episodes (NR-PM<sub>1</sub> reaching up to 68 µg m<sup>-3</sup> over a 30-min period).

PM<sub>1</sub> concentrations were on average 8.2 µg m<sup>-3</sup> representing 11% of PM<sub>10</sub>, and were dominated by NR species (71%) with minor contributions of absorbing species (9%). The remaining unaccounted fraction (20% on average, up to 75% during identified dust events) was mainly attributed to mineral dust, strongly suggesting a minor contribution of sea salt in the submicron fraction. Fe concentrations (5%) obtained from the deconvolution of absorption measurements were consistent with the dust events observed on site. Among the species identified in the PM<sub>1</sub> fraction, sulfate and organics represented 32 and 31%, respectively, followed by ammonium 14%, nitrate 9%, BC 5%, Fe 9% and Chl <1%. OM dominated the NR-PM<sub>1</sub> fraction when the sampling site was under continental air mass influences (north-eastern winds), whereas marine air masses (from western winds) preferentially brought higher concentrations of sulfate species on site.

Source apportionment of the organic fraction allowed to identify four types of OA. The organic fraction is composed of a highly-oxidized OOA (45%), whose regional origin is underlined by its important contribution to the organic fraction during marine days (62%) but also by its increasing concentration during daytime with a maximum under sea breeze influence. Nonetheless, its higher correlation with NO<sub>3</sub> as well as morning and evening peaks observed for continental and sea breeze daily profiles tend to associate it partially to direct emissions or fast oxidation processes of anthropogenic compounds. Three primary OA linked to anthropogenic activities from nearby sources were also identified: HOA (22%), COA (28%) and a new factor LCOA (3%) related to local combustion sources (emissions from open-waste burning and fish smoking areas), for which a good correlation with particulate chloride (m/z 36) was consistently found. Non-refractory chloride fragments from waste burning or fish smoking areas were suggested to originate from local plastic smoldering/flaming processes (for the former) and/or sea salt (for both) submitted to high temperatures under continental influence. This factor, although minor on average, could represent as high as 7% on a 30-minute time period when the air masses were blowing from the local waste burning areas, and very likely resulted in the concomitant emissions of highly-toxic compounds such as dioxins that would require further investigation. Back-trajectories also suggest possible distant sources of combustion, with part of LCOA, OOA and BC associated to processed oceanic air masses which could be influenced by Dakar traffic emissions and waste burning activities, as well as shipping emissions along the West African coast.

Overall, our study suggests that natural sources strongly influence PM<sub>1</sub> levels in M'Bour, mainly due to the large influence of marine conditions associated with high sulfate levels, and additional significant influence of desert dust. Our measurements carried out at a suburban site away from megacities allowed to provide new insight into the complex mixture between local anthropogenic sources and regional background aerosols in the PM<sub>1</sub> fraction in West Africa at the end of the dry season.

As shown during this field campaign, at least half of the organic aerosols measured in the submicron fraction are from anthropogenic origins (HOA + COA + LCOA) and we were able to attribute them to specific sources. On the contrary, little is known about the oxygenated fraction – often associated to secondary organic aerosols, which constitutes the other half of OA and therefore efforts should be directed toward better characterizing SOA precursors

(anthropogenic and biogenic) and their concentration levels in West Africa. Moreover, the specific LCOA source puts an emphasis on open waste burning, which is highly problematic in terms of health issues, and should be addressed through the implementation of waste disposal facilities and an effective waste collection infrastructure.

### Data availability

- 5 Data from ACSM and aethalometer instruments are available upon request to the corresponding author, V. Riffault. PM<sub>10</sub> data can be accessed by request to A. Féron (LISA).

### Acknowledgements

- 10 LHR's PhD grant and the SHADOW campaign are financially supported by the CaPPA project (Chemical and Physical Properties of the Atmosphere), which is funded by the French National Research Agency (ANR) through the PIA (*Programme d'Investissement d'Avenir*) under contract "ANR-11-LABX-0005-01", by the Regional Council "Hauts-de-France" and the European Regional Development Fund (ERDF).

### References

- 15 Bond, T. C. and Bergstrom, R. W.: Light Absorption by Carbonaceous Particles: An Investigative Review, *Aerosol Sci. Technol.*, 40(1), 27–67, doi:10.1080/02786820500421521, 2006.
- Bovchaliuk, V., Podvin, T., Mortier, A., Goloub, P., Dubovik, O., Tanré, D., Veselovskii, I. and Victori, S.: Aerosol optical and microphysical properties retrieved from combination LIDAR with sun/sky photometer: preliminary results over Lille, *Data Process.*, 4, 02, 2014.
- 20 Brauer, M., Amann, M., Burnett, R. T., Cohen, A., Dentener, F., Ezzati, M., Henderson, S. B., Krzyzanowski, M., Martin, R. V., Van Dingenen, R., van Donkelaar, A. and Thurston, G. D.: Exposure Assessment for Estimation of the Global Burden of Disease Attributable to Outdoor Air Pollution, *Environ. Sci. Technol.*, 46(2), 652–660, doi:10.1021/es2025752, 2012.
- 25 Bressi, M., Cavalli, F., Belis, C. A., Putaud, J.-P., Fröhlich, R., Martins dos Santos, S., Petralia, E., Prévôt, A. S. H., Berico, M., Malaguti, A. and Canonaco, F.: Variations in the chemical composition of the submicron aerosol and in the sources of the organic fraction at a regional background site of the Po Valley (Italy), *Atmos Chem Phys*, 16(20), 12875–12896, doi:10.5194/acp-16-12875-2016, 2016.
- 30 Brook, R. D., Franklin, B., Cascio, W., Hong, Y., Howard, G., Lipsett, M., Luepker, R., Mittleman, M., Samet, J. and Smith, S. C.: Air pollution and cardiovascular disease A statement for healthcare professionals from the expert panel on population and prevention science of the American Heart Association, *Circulation*, 109(21), 2655–2671, 2004.
- 35 Budisulistiorini, S. H., Canagaratna, M. R., Croteau, P. L., Baumann, K., Edgerton, E. S., Kollman, M. S., Ng, N. L., Verma, V., Shaw, S. L., Knipping, E. M., Worsnop, D. R., Jayne, J. T., Weber, R. J. and Surratt, J. D.: Intercomparison of an Aerosol Chemical Speciation Monitor (ACSM) with ambient fine aerosol measurements in downtown Atlanta, Georgia, *Atmos Meas Tech*, 7(7), 1929–1941, doi:10.5194/amt-7-1929-2014, 2014.
- Canagaratna, M. R., Jayne, J. T., Jimenez, J. L., Allan, J. D., Alfarra, M. R., Zhang, Q., Onasch, T. B., Drewnick, F., Coe, H., Middlebrook, A., Delia, A., Williams, L. R., Trimborn, A. M., Northway, M. J., DeCarlo, P. F., Kolb, C. E.,

- Davidovits, P. and Worsnop, D. R.: Chemical and microphysical characterization of ambient aerosols with the aerodyne aerosol mass spectrometer, *Mass Spectrom. Rev.*, 26(2), 185–222, doi:10.1002/mas.20115, 2007.
- Canonaco, F., Crippa, M., Slowik, J. G., Baltensperger, U. and Prévôt, A. S. H.: SoFi, an IGOR-based interface for the efficient use of the generalized multiline engine (ME-2) for the source apportionment: ME-2 application to aerosol mass spectrometer data, *Atmos Meas Tech*, 6(12), 3649–3661, doi:10.5194/amt-6-3649-2013, 2013.
- Charlson, R. J., Lovelock, J. E., Andreae, M. O. and Warren, S. G.: Oceanic phytoplankton, atmospheric sulphur, cloud albedo and climate, *Nature*, 326(6114), 655–661, 1987.
- Chiapello, I., Bergametti, G., Gomes, L., Chatenet, B., Dulac, F., Pimenta, J. and Soares, E. S.: An additional low layer transport of Sahelian and Saharan dust over the north-eastern Tropical Atlantic, *Geophys. Res. Lett.*, 22(23), 3191–3194, doi:10.1029/95GL03313, 1995.
- Chou, C., Formenti, P., Maille, M., Ausset, P., Helas, G., Harrison, M. and Osborne, S.: Size distribution, shape, and composition of mineral dust aerosols collected during the African Monsoon Multidisciplinary Analysis Special Observation Period 0: Dust and Biomass-Burning Experiment field campaign in Niger, January 2006, *J. Geophys. Res. Atmospheres*, 113(D23), D00C10, doi:10.1029/2008JD009897, 2008.
- Crenn, V., Sciare, J., Croteau, P. L., Verlhac, S., Fröhlich, R., Belis, C. A., Aas, W., Äijälä, M., Alastuey, A., Artiñano, B., Baisnée, D., Bonnaire, N., Bressi, M., Canagaratna, M., Canonaco, F., Carbone, C., Cavalli, F., Coz, E., Cubison, M. J., Esser-Gietl, J. K., Green, D. C., Gros, V., Heikkinen, L., Herrmann, H., Lunder, C., Minguillón, M. C., Močnik, G., O'Dowd, C. D., Ovadnevaite, J., Petit, J.-E., Petralia, E., Poulain, L., Priestman, M., Riffault, V., Ripoll, A., Sarda-Estève, R., Slowik, J. G., Setyan, A., Wiedensohler, A., Baltensperger, U., Prévôt, A. S. H., Jayne, J. T. and Favez, O.: ACTRIS ACSM intercomparison – Part 1: Reproducibility of concentration and fragment results from 13 individual Quadrupole Aerosol Chemical Speciation Monitors (Q-ACSM) and consistency with co-located instruments, *Atmos Meas Tech*, 8(12), 5063–5087, doi:10.5194/amt-8-5063-2015, 2015.
- Crippa, M., El Haddad, I., Slowik, J. G., DeCarlo, P. F., Mohr, C., Heringa, M. F., Chirico, R., Marchand, N., Sciare, J. and Baltensperger, U.: Identification of marine and continental aerosol sources in Paris using high resolution aerosol mass spectrometry, *J. Geophys. Res. Atmospheres*, 118(4), 1950–1963, 2013.
- Cubison, M. J., Ortega, A. M., Hayes, P. L., Farmer, D. K., Day, D., Lechner, M. J., Brune, W. H., Apel, E., Diskin, G. S., Fisher, J. A., Fuelberg, H. E., Hecobian, A., Knapp, D. J., Mikoviny, T., Riemer, D., Sachse, G. W., Sessions, W., Weber, R. J., Weinheimer, A. J., Wisthaler, A. and Jimenez, J. L.: Effects of aging on organic aerosol from open biomass burning smoke in aircraft and laboratory studies, *Atmos Chem Phys*, 11(23), 12049–12064, doi:10.5194/acp-11-12049-2011, 2011.
- Deboudt, K., Flament, P., Choël, M., Gloter, A., Sobanska, S. and Colliex, C.: Mixing state of aerosols and direct observation of carbonaceous and marine coatings on African dust by individual particle analysis, *J. Geophys. Res. Atmospheres*, 115(D24), D24207, doi:10.1029/2010jd013921, 2010.
- Derimian, Y., Léon, J.-F., Dubovik, O., Chiapello, I., Tanré, D., Sinyuk, A., Auriol, F., Podvin, T., Brogniez, G. and Holben, B. N.: Radiative properties of aerosol mixture observed during the dry season 2006 over M'Bour, Senegal (African Monsoon Multidisciplinary Analysis campaign), *J. Geophys. Res. Atmospheres*, 113(D23), D00C09, doi:10.1029/2008JD009904, 2008.
- Doumbia, E. H. T., Lioussé, C., Galy-Lacaux, C., Ndiaye, S. A., Diop, B., Ouafu, M., Assamoi, E. M., Gardrat, E., Castera, P., Rosset, R., Akpo, A. and Sigha, L.: Real time black carbon measurements in West and Central Africa urban sites, *Atmos. Environ.*, 54, 529–537, doi:10.1016/j.atmosenv.2012.02.005, 2012.
- Drinovec, L., Močnik, G., Zotter, P., Prévôt, A. S. H., Ruckstuhl, C., Coz, E., Rupakheti, M., Sciare, J., Müller, T., Wiedensohler, A. and Hansen, A. D. A.: The “dual-spot” Aethalometer: an improved measurement of aerosol black carbon with real-time loading compensation, *Atmos Meas Tech*, 8(5), 1965–1979, doi:10.5194/amt-8-1965-2015, 2015.

- Du, W., Sun, Y. L., Xu, Y. S., Jiang, Q., Wang, Q. Q., Yang, W., Wang, F., Bai, Z. P., Zhao, X. D. and Yang, Y. C.: Chemical characterization of submicron aerosol and particle growth events at a national background site (3295 m a.s.l.) in the Tibetan Plateau, *Atmos Chem Phys Discuss*, 15(9), 13515–13550, doi:10.5194/acpd-15-13515-2015, 2015.
- 5 Fialho, P., Hansen, A. D. A. and Honrath, R. E.: Absorption coefficients by aerosols in remote areas: a new approach to decouple dust and black carbon absorption coefficients using seven-wavelength Aethalometer data, *J. Aerosol Sci.*, 36(2), 267–282, doi:10.1016/j.jaerosci.2004.09.004, 2005.
- Fialho, P., Freitas, M. C., Barata, F., Vieira, B., Hansen, A. D. A. and Honrath, R. E.: The Aethalometer calibration and determination of iron concentration in dust aerosols, *J. Aerosol Sci.*, 37(11), 1497–1506, doi:10.1016/j.jaerosci.2006.03.002, 2006.
- 10 Fialho, P., Cerqueira, M., Pio, C., Cardoso, J., Nunes, T., Custódio, D., Alves, C., Almeida, S. M., Almeida-Silva, M., Reis, M. and Rocha, F.: The application of a multi-wavelength Aethalometer to estimate iron dust and black carbon concentrations in the marine boundary layer of Cape Verde, *Atmos. Environ.*, 97, 136–143, doi:10.1016/j.atmosenv.2014.08.008, 2014.
- 15 Fitzgerald, J. W.: Marine aerosols: A review, *Atmospheric Environ. Part Gen. Top.*, 25(3–4), 533–545, doi:10.1016/0960-1686(91)90050-H, 1991.
- Flament, P., Deboudt, K., Cachier, H., Châtenet, B. and Mériaux, X.: Mineral dust and carbonaceous aerosols in West Africa: Source assessment and characterization, *Atmos. Environ.*, 45(22), 3742–3749, doi:10.1016/j.atmosenv.2011.04.013, 2011.
- 20 Fomba, K. W., Müller, K., van Pinxteren, D., Poulain, L., van Pinxteren, M. and Herrmann, H.: Long-term chemical characterization of tropical and marine aerosols at the Cape Verde Atmospheric Observatory (CVAO) from 2007 to 2011, *Atmospheric Chem. Phys.*, 14(17), 8883–8904, doi:10.5194/acp-14-8883-2014, 2014.
- Formenti, P., Rajot, J. L., Desboeufs, K., Caqueneau, S., Chevaillier, S., Nava, S., Gaudichet, A., Journet, E., Triquet, S., Alfaro, S., Chiari, M., Haywood, J., Coe, H. and Highwood, E.: Regional variability of the composition of mineral dust from western Africa: Results from the AMMA SOP0/DABEX and DODO field campaigns, *J. Geophys. Res. Atmospheres*, 113(D23), D00C13, doi:10.1029/2008jd009903, 2008a.
- 25 Formenti, P., Rajot, J. L., Desboeufs, K., Caqueneau, S., Chevaillier, S., Nava, S., Gaudichet, A., Journet, E., Triquet, S., Alfaro, S., Chiari, M., Haywood, J., Coe, H. and Highwood, E.: Regional variability of the composition of mineral dust from western Africa: Results from the AMMA SOP0/DABEX and DODO field campaigns, *J. Geophys. Res. Atmospheres*, 113(D23), D00C13, doi:10.1029/2008JD009903, 2008b.
- 30 Fröhlich, R., Cubison, M. J., Slowik, J. G., Bukowiecki, N., Canonaco, F., Croteau, P. L., Gysel, M., Henne, S., Herrmann, E., Jayne, J. T., Steinbacher, M., Worsnop, D. R., Baltensperger, U. and Prévôt, A. S. H.: Fourteen months of on-line measurements of the non-refractory submicron aerosol at the Jungfraujoch (3580 m a.s.l.) – chemical composition, origins and organic aerosol sources, *Atmos Chem Phys*, 15(19), 11373–11398, doi:10.5194/acp-15-11373-2015, 2015.
- 35 Grover, B. D., Kleinman, M., Eatough, N. L., Eatough, D. J., Hopke, P. K., Long, R. W., Wilson, W. E., Meyer, M. B. and Ambs, J. L.: Measurement of total PM<sub>2.5</sub> mass (nonvolatile plus semivolatile) with the Filter Dynamic Measurement System tapered element oscillating microbalance monitor, *J. Geophys. Res. Atmospheres*, 110(D7), D07S03, doi:10.1029/2004JD004995, 2005.
- 40 Gullett, B. K., Lemieux, P. M., Lutes, C. C., Winterrowd, C. K. and Winters, D. L.: Emissions of PCDD/F from uncontrolled, domestic waste burning, *Chemosphere*, 43(4–7), 721–725, doi:10.1016/S0045-6535(00)00425-2, 2001.
- Hallquist, M., Wenger, J. C., Baltensperger, U., Rudich, Y., Simpson, D., Claeys, M., Dommen, J., Donahue, N. M., George, C., Goldstein, A. H., Hamilton, J. F., Herrmann, H., Hoffmann, T., Iinuma, Y., Jang, M., Jenkin, M. E., Jimenez, J. L., Kiendler-Scharr, A., Maenhaut, W., McFiggans, G., Mentel, T. F., Monod, A., Prévôt, A. S. H.,



- Seinfeld, J. H., Surratt, J. D., Szmigielski, R. and Wildt, J.: The formation, properties and impact of secondary organic aerosol: current and emerging issues, *Atmospheric Chem. Phys.*, 9(14), 5155–5236, doi:10.5194/acp-9-5155-2009, 2009.
- Hand, V. L., Capes, G., Vaughan, D. J., Formenti, P., Haywood, J. M. and Coe, H. C. D.: Evidence of internal mixing of African dust and biomass burning particles by individual particle analysis using electron beam techniques, *J. Geophys. Res. Atmospheres*, 115(D13), n/a-n/a, doi:10.1029/2009jd012938, 2010.
- Haywood, J. M., Pelon, J., Formenti, P., Bharmal, N., Brooks, M., Capes, G., Chazette, P., Chou, C., Christopher, S., Coe, H., Cuesta, J., Derimian, Y., Desboeufs, K., Greed, G., Harrison, M., Heese, B., Highwood, E. J., Johnson, B., Mallet, M., Marticorena, B., Marsham, J., Milton, S., Myhre, G., Osborne, S. R., Parker, D. J., Rajot, J. L., Schulz, M., Slingo, A., Tanré, D. and Tulet, P.: Overview of the Dust and Biomass-burning Experiment and African Monsoon Multidisciplinary Analysis Special Observing Period-0, *J. Geophys. Res. Atmospheres*, 113(D23), D00C17, doi:10.1029/2008jd010077, 2008.
- Hennigan, C. J., Sullivan, A. P., Collett, J. L. and Robinson, A. L.: Levoglucosan stability in biomass burning particles exposed to hydroxyl radicals, *Geophys. Res. Lett.*, 37(9), L09806, doi:10.1029/2010GL043088, 2010.
- Holben, B. N., Eck, T. F., Slutsker, I., Tanré, D., Buis, J. P., Setzer, A., Vermote, E., Reagan, J. A., Kaufman, Y. J., Nakajima, T., Lavenu, F., Jankowiak, I. and Smirnov, A.: AERONET—A Federated Instrument Network and Data Archive for Aerosol Characterization, *Remote Sens. Environ.*, 66(1), 1–16, doi:10.1016/S0034-4257(98)00031-5, 1998.
- Ianniello, A., Spataro, F., Esposito, G., Allegrini, I., Hu, M. and Zhu, T.: Chemical characteristics of inorganic ammonium salts in PM<sub>2.5</sub> in the atmosphere of Beijing (China), *Atmospheric Chem. Phys.*, 11(21), 10803–10822, doi:10.5194/acp-11-10803-2011, 2011.
- IPCC: Climate change 2007-the physical science basis: Working group I contribution to the fourth assessment report of the IPCC, Cambridge University Press., 2007.
- IPCC: Climate Change 2013: The Physical Science Basis: Working Group I Contribution to the Fifth Assessment Report of the Intergovernmental Panel on Climate Change, Cambridge University Press., 2013.
- Joshi, N., Romanias, M., Riffault, V. and Thévenet, F.: Investigating water adsorption on natural mineral dust particles: A DRIFT and BET theory study, submitted to Aeolian Research, 2017.
- Kaly, F., Marticorena, B., Chatenet, B., Rajot, J. L., Janicot, S., Niang, A., Yahi, H., Thiria, S., Maman, A., Zakou, A., Coulibaly, B. S., Coulibaly, M., Koné, I., Traoré, S., Diallo, A. and Ndiaye, T.: Variability of mineral dust concentrations over West Africa monitored by the Sahelian Dust Transect, *Atmospheric Res.*, 164–165, 226–241, doi:10.1016/j.atmosres.2015.05.011, 2015.
- Karol, Y., Tanré, D., Goloub, P., Ververde, C., Balois, J. Y., Blarel, L., Podvin, T., Mortier, A. and Chaikovsky, A.: Airborne sun photometer PLASMA: concept, measurements, comparison of aerosol extinction vertical profile with lidar, *Atmos Meas Tech*, 6(9), 2383–2389, doi:10.5194/amt-6-2383-2013, 2013.
- Kelly, F. J. and Fussell, J. C.: Size, source and chemical composition as determinants of toxicity attributable to ambient particulate matter, *Atmos. Environ.*, 60, 504–526, 2012.
- Lafon, S., Sokolik, I. N., Rajot, J. L., Caqueneau, S. and Gaudichet, A.: Characterization of iron oxides in mineral dust aerosols: Implications for light absorption, *J. Geophys. Res. Atmospheres*, 111(D21), D21207, doi:10.1029/2005JD007016, 2006.
- Lanz, V. A., Prévôt, A. S. H., Alfarra, M. R., Weimer, S., Mohr, C., DeCarlo, P. F., Gianini, M. F. D., Hueglin, C., Schneider, J., Favez, O., D’Anna, B., George, C. and Baltensperger, U.: Characterization of aerosol chemical

- composition with aerosol mass spectrometry in Central Europe: an overview, *Atmos Chem Phys*, 10(21), 10453–10471, doi:10.5194/acp-10-10453-2010, 2010.
- Lemieux, P. M., Lutes, C. C. and Santoianni, D. A.: Emissions of organic air toxics from open burning: a comprehensive review, *Prog. Energy Combust. Sci.*, 30(1), 1–32, doi:10.1016/j.pecs.2003.08.001, 2004.
- 5 Léon, J.-F., Derimian, Y., Chiapello, I., Tanré, D., Podvin, T., Chatenet, B., Diallo, A. and Deroo, C.: Aerosol vertical distribution and optical properties over M'Bour (16.96° W; 14.39° N), Senegal from 2006 to 2008, *Atmos Chem Phys*, 9(23), 9249–9261, doi:10.5194/acp-9-9249-2009, 2009.
- Lioussé, C., Guillaume, B., Grégoire, J. M., Mallet, M., Galy, C., Pont, V., Akpo, A., Bedou, M., Castéra, P., Dungall, L., Gardrat, E., Granier, C., Konar, A., Malavelle, F., Mariscal, A., Mieville, A., Rosset, R., Serça, D.,  
 10 Solmon, F., Tummon, F., Assamoi, E., Yoboué, V. and Van Velthoven, P.: Updated African biomass burning emission inventories in the framework of the AMMA-IDAF program, with an evaluation of combustion aerosols, *Atmos Chem Phys*, 10(19), 9631–9646, doi:10.5194/acp-10-9631-2010, 2010.
- Marticorena, B., Chatenet, B., Rajot, J. L., Traoré, S., Coulibaly, M., Diallo, A., Koné, I., Maman, A., Ndiaye, T. and Zakou, A.: Temporal variability of mineral dust concentrations over West Africa: analyses of a pluriannual  
 15 monitoring from the AMMA Sahelian Dust Transect, *Atmos Chem Phys*, 10(18), 8899–8915, doi:10.5194/acp-10-8899-2010, 2010.
- Martiny, N. and Chiapello, I.: Assessments for the impact of mineral dust on the meningitis incidence in West Africa, *Atmos. Environ.*, 70(0), 245–253, doi:10.1016/j.atmosenv.2013.01.016, 2013.
- McCulloch, A., Aucott, M. L., Benkovitz, C. M., Graedel, T. E., Kleiman, G., Midgley, P. M. and Li, Y.-F.: Global  
 20 emissions of hydrogen chloride and chloromethane from coal combustion, incineration and industrial activities: Reactive Chlorine Emissions Inventory, *J. Geophys. Res. Atmospheres*, 104(D7), 8391–8403, doi:10.1029/1999JD900025, 1999.
- Middlebrook, A. M., Bahreini, R., Jimenez, J. L. and Canagaratna, M. R.: Evaluation of Composition-Dependent Collection Efficiencies for the Aerodyne Aerosol Mass Spectrometer using Field Data, *Aerosol Sci. Technol.*, 46(3),  
 25 258–271, doi:10.1080/02786826.2011.620041, 2012.
- Milic, A., Mallet, M. D., Cravigan, L. T., Alroe, J., Ristovski, Z. D., Selleck, P., Lawson, S. J., Ward, J., Desservettaz, M. J., Paton-Walsh, C., Williams, L. R., Keywood, M. D. and Miljevic, B.: Aging of aerosols emitted from biomass burning in northern Australia, *Atmos Chem Phys Discuss*, 2016, 1–24, doi:10.5194/acp-2016-730, 2016.
- 30 Minguillón, M., Ripoll, A., Pérez, N., Prévôt, A., Canonaco, F., Querol, X. and Alastuey, A.: Chemical characterization of submicron regional background aerosols in the Western Mediterranean using an Aerosol Chemical Speciation Monitor, *Atmospheric Chem. Phys. Discuss.*, 15(1), 965–1000, 2015.
- Mohr, C., DeCarlo, P. F., Heringa, M. F., Chirico, R., Slowik, J. G., Richter, R., Reche, C., Alastuey, A., Querol, X., Seco, R., Peñuelas, J., Jiménez, J. L., Crippa, M., Zimmermann, R., Baltensperger, U. and Prévôt, A. S. H.:  
 35 Identification and quantification of organic aerosol from cooking and other sources in Barcelona using aerosol mass spectrometer data, *Atmos Chem Phys*, 12(4), 1649–1665, doi:10.5194/acp-12-1649-2012, 2012.
- Moreno, T., Querol, X., Castillo, S., Alastuey, A., Cuevas, E., Herrmann, L., Mounkaila, M., Elvira, J. and Gibbons, W.: Geochemical variations in aeolian mineral particles from the Sahara–Sahel Dust Corridor, *Chemosphere*, 65(2), 261–270, doi:10.1016/j.chemosphere.2006.02.052, 2006.
- 40 Ng, N. L., Herndon, S. C., Trimborn, A., Canagaratna, M. R., Croteau, P. L., Onasch, T. B., Sueper, D., Worsnop, D. R., Zhang, Q., Sun, Y. L. and Jayne, J. T.: An Aerosol Chemical Speciation Monitor (ACSM) for Routine Monitoring of the Composition and Mass Concentrations of Ambient Aerosol, *Aerosol Sci. Technol.*, 45(7), 780–794, doi:10.1080/02786826.2011.560211, 2011a.

- Ng, N. L., Canagaratna, M. R., Jimenez, J. L., Zhang, Q., Ulbrich, I. M. and Worsnop, D. R.: Real-Time Methods for Estimating Organic Component Mass Concentrations from Aerosol Mass Spectrometer Data, *Environ. Sci. Technol.*, 45(3), 910–916, doi:10.1021/es102951k, 2011b.
- 5 Nuaaman, I., Li, S.-M., Hayden, K. L., Onasch, T. B., Massoli, P., Sueper, D., Worsnop, D. R., Bates, T. S., Quinn, P. K. and McLaren, R.: Separating refractory and non-refractory particulate chloride and estimating chloride depletion by aerosol mass spectrometry in a marine environment, *Atmos Chem Phys Discuss*, 15(2), 2085–2118, doi:10.5194/acpd-15-2085-2015, 2015.
- 10 Osborne, S. R., Johnson, B. T., Haywood, J. M., Baran, A. J., Harrison, M. A. J. and McConnell, C. L.: Physical and optical properties of mineral dust aerosol during the Dust and Biomass-burning Experiment, *J. Geophys. Res. Atmospheres*, 113(D23), D00C03, doi:10.1029/2007jd009551, 2008.
- Ovadnevaite, J., Ceburnis, D., Canagaratna, M., Berresheim, H., Bialek, J., Martucci, G., Worsnop, D. R. and O'Dowd, C.: On the effect of wind speed on submicron sea salt mass concentrations and source fluxes, *J. Geophys. Res. Atmospheres*, 117(D16), D16201, doi:10.1029/2011JD017379, 2012.
- 15 Paatero, P. and Tapper, U.: Positive matrix factorization: A non-negative factor model with optimal utilization of error estimates of data values, *Environmetrics*, 5(2), 111–126, doi:10.1002/env.3170050203, 1994.
- Paris, R., Desboeufs, K. V., Formenti, P., Nava, S. and Chou, C.: Chemical characterisation of iron in dust and biomass burning aerosols during AMMA-SOP0/DABEX: implication for iron solubility, *Atmospheric Chem. Phys.*, 10(9), 4273–4282, doi:10.5194/acp-10-4273-2010, 2010.
- 20 Parworth, C., Fast, J., Mei, F., Shippert, T., Sivaraman, C., Tilp, A., Watson, T. and Zhang, Q.: Long-term measurements of submicrometer aerosol chemistry at the Southern Great Plains (SGP) using an Aerosol Chemical Speciation Monitor (ACSM), *Atmos. Environ.*, 106, 43–55, doi:10.1016/j.atmosenv.2015.01.060, 2015.
- Petit, J.-E., Favez, O., Sciare, J., Canonaco, F., Croteau, P., Močnik, G., Jayne, J., Worsnop, D. and Leoz-Garziandia, E.: Submicron aerosol source apportionment of wintertime pollution in Paris, France by double positive matrix factorization (PMF2) using an aerosol chemical speciation monitor (ACSM) and a multi-wavelength Aethalometer, 25 *Atmos Chem Phys*, 14(24), 13773–13787, doi:10.5194/acp-14-13773-2014, 2014.
- Petit, J.-E., Favez, O., Sciare, J., Crenn, V., Sarda-Estève, R., Bonnaire, N., Močnik, G., Dupont, J.-C., Haeffelin, M. and Leoz-Garziandia, E.: Two years of near real-time chemical composition of submicron aerosols in the region of Paris using an Aerosol Chemical Speciation Monitor (ACSM) and a multi-wavelength Aethalometer, *Atmos Chem Phys*, 15(6), 2985–3005, doi:10.5194/acp-15-2985-2015, 2015.
- 30 Pio, C. A., Cardoso, J., Cerqueira, M. A., Calvo, A., Nunes, T. V., Alves, C. A., Custodio, D., Almeida, S. M. and Silva, M. A.: Seasonal variability of aerosol concentration and size distribution in Cape Verde using a continuous aerosol optical spectrometer, *Front. Environ. Sci.*, 2, doi:10.3389/fenvs.2014.00015, 2014.
- Prenni, A. J., Day, D. E., Evanowski-Cole, A. R., Sive, B. C., Hecobian, A., Zhou, Y., Gebhart, K. A., Hand, J. L., Sullivan, A. P., Li, Y., Schurman, M. I., Desyaterik, Y., Malm, W. C., Collett Jr., J. L. and Schichtel, B. A.: Oil and gas impacts on air quality in federal lands in the Bakken region: an overview of the Bakken Air Quality Study and first results, *Atmos Chem Phys*, 16(3), 1401–1416, doi:10.5194/acp-16-1401-2016, 2016.
- 35 Redelsperger, J.-L., Thorncroft, C. D., Diedhiou, A., Lebel, T., Parker, D. J. and Polcher, J.: African Monsoon Multidisciplinary Analysis: An International Research Project and Field Campaign, *Bull. Am. Meteorol. Soc.*, 87(12), 1739–1746, doi:10.1175/BAMS-87-12-1739, 2006.
- 40 Ripoll, A., Minguillón, M. C., Pey, J., Jimenez, J. L., Day, D. A., Sosedova, Y., Canonaco, F., Prévôt, A. S. H., Querol, X. and Alastuey, A.: Long-term real-time chemical characterization of submicron aerosols at Montsec (southern Pyrenees, 1570 m a.s.l.), *Atmos Chem Phys*, 15(6), 2935–2951, doi:10.5194/acp-15-2935-2015, 2015.

- Robinson, A. L., Donahue, N. M., Shrivastava, M. K., Weitkamp, E. A., Sage, A. M., Grieshop, A. P., Lane, T. E., Pierce, J. R. and Pandis, S. N.: Rethinking Organic Aerosols: Semivolatile Emissions and Photochemical Aging, *Science*, 315(5816), 1259–1262, doi:10.1126/science.1133061, 2007.
- Salcedo, D., Onasch, T. B., Dzepina, K., Canagaratna, M. R., Zhang, Q., Huffman, J. A., DeCarlo, P. F., Jayne, J. T.,  
5 Mortimer, P., Worsnop, D. R., Kolb, C. E., Johnson, K. S., Zuberi, B., Marr, L. C., Volkamer, R., Molina, L. T.,  
Molina, M. J., Cardenas, B., Bernabé, R. M., Márquez, C., Gaffney, J. S., Marley, N. A., Laskin, A., Shutthanandan,  
V., Xie, Y., Brune, W., Leshner, R., Shirley, T. and Jimenez, J. L.: Characterization of ambient aerosols in Mexico  
City during the MCMA-2003 campaign with Aerosol Mass Spectrometry: results from the CENICA Supersite,  
*Atmos Chem Phys*, 6(4), 925–946, doi:10.5194/acp-6-925-2006, 2006.
- 10 Schlag, P., Kiendler-Scharr, A., Blom, M. J., Canonaco, F., Henzing, J. S., Moerman, M. M., Prévôt, A. S. H. and  
Holzinger, R.: Aerosol source apportionment from 1 year measurements at the CESAR tower at Cabauw, NL, *Atmos  
Chem Phys Discuss*, 15(23), 35117–35155, doi:10.5194/acpd-15-35117-2015, 2015.
- Schurman, M. I., Lee, T., Desyaterik, Y., Schichtel, B. A., Kreidenweis, S. M. and Collett Jr., J. L.: Transport,  
biomass burning, and in-situ formation contribute to fine particle concentrations at a remote site near Grand Teton  
15 National Park, *Atmos. Environ.*, 112, 257–268, doi:10.1016/j.atmosenv.2015.04.043, 2015.
- Slingo, A., Bharmal, N. A., Robinson, G. J., Settle, J. J., Allan, R. P., White, H. E., Lamb, P. J., Lélé, M. I., Turner,  
D. D., McFarlane, S., Kassianov, E., Barnard, J., Flynn, C. and Miller, M.: Overview of observations from the  
RADAGAST experiment in Niamey, Niger: Meteorology and thermodynamic variables, *J. Geophys. Res.  
Atmospheres*, 113(D13), D00E01, doi:10.1029/2008JD009909, 2008.
- 20 Sun, C., Lee, B. P., Huang, D., Jie Li, Y., Schurman, M. I., Louie, P. K. K., Luk, C. and Chan, C. K.: Continuous  
measurements at the urban roadside in an Asian megacity by Aerosol Chemical Speciation Monitor (ACSM):  
particulate matter characteristics during fall and winter seasons in Hong Kong, *Atmos Chem Phys*, 16(3), 1713–  
1728, doi:10.5194/acp-16-1713-2016, 2016.
- Sun, Y., Wang, Z., Dong, H., Yang, T., Li, J., Pan, X., Chen, P. and Jayne, J. T.: Characterization of summer organic  
25 and inorganic aerosols in Beijing, China with an Aerosol Chemical Speciation Monitor, *Atmos. Environ.*, 51(0),  
250–259, doi:10.1016/j.atmosenv.2012.01.013, 2012.
- Sun, Y. L., Wang, Z. F., Fu, P. Q., Yang, T., Jiang, Q., Dong, H. B., Li, J. and Jia, J. J.: Aerosol composition, sources  
and processes during wintertime in Beijing, China, *Atmospheric Chem. Phys.*, 13(9), 4577–4592, doi:10.5194/acp-  
13-4577-2013, 2013.
- 30 Tiitta, P., Vakkari, V., Croteau, P., Beukes, J. P., van Zyl, P. G., Josipovic, M., Venter, A. D., Jaars, K., Pienaar, J. J.,  
Ng, N. L., Canagaratna, M. R., Jayne, J. T., Kerminen, V. M., Kokkola, H., Kulmala, M., Laaksonen, A., Worsnop,  
D. R. and Laakso, L.: Chemical composition, main sources and temporal variability of PM1 aerosols in southern  
African grassland, *Atmos Chem Phys*, 14(4), 1909–1927, doi:10.5194/acp-14-1909-2014, 2014.
- Titos, G., Lyamani, H., Pandolfi, M., Alastuey, A. and Alados-Arboledas, L.: Identification of fine (PM1) and coarse  
35 (PM10-1) sources of particulate matter in an urban environment, *Atmos. Environ.*, 89(0), 593–602,  
doi:10.1016/j.atmosenv.2014.03.001, 2015.
- Topping, D., Coe, H., McFiggans, G., Burgess, R., Allan, J., Alfarra, M. R., Bower, K., Choularton, T. W., Decesari,  
S. and Facchini, M. C.: Aerosol chemical characteristics from sampling conducted on the Island of Jeju, Korea  
during ACE Asia, *Atmos. Environ.*, 38(14), 2111–2123, doi:10.1016/j.atmosenv.2004.01.022, 2004.
- 40 Tue, N. M., Goto, A., Takahashi, S., Itai, T., Asante, K. A., Kunisue, T. and Tanabe, S.: Release of chlorinated,  
brominated and mixed halogenated dioxin-related compounds to soils from open burning of e-waste in Agbogbloshie  
(Accra, Ghana), *J. Hazard. Mater.*, 302, 151–157, doi:10.1016/j.jhazmat.2015.09.062, 2016.
- Val, S., Liousse, C., Doumbia, E. H. T., Galy-Lacaux, C., Cachier, H., Marchand, N., Badel, A., Gardrat, E.,  
Sylvestre, A. and Baeza-Squiban, A.: Physico-chemical characterization of African urban aerosols (Bamako in Mali

and Dakar in Senegal) and their toxic effects in human bronchial epithelial cells: description of a worrying situation, *Part Fibre Toxicol*, 10(10), 2013.

- 5 Veselovskii, I., Goloub, P., Podvin, T., Bovchaliuk, V., Derimian, Y., Augustin, P., Fourmentin, M., Tanre, D., Korenskiy, M., Whiteman, D. N., Diallo, A., Ndiaye, T., Kolgotin, A. and Dubovik, O.: Study of African Dust with multi-wavelength Raman Lidar during the “SHADOW” campaign in Senegal, *Atmospheric Chem. Phys. Discuss.*, 1–40, doi:10.5194/acp-2016-109, 2016.
- Von der Weiden, S.-L., Drewnick, F. and Borrmann, S.: Particle Loss Calculator – a new software tool for the assessment of the performance of aerosol inlet systems, *Atmos Meas Tech*, 2(2), 479–494, doi:10.5194/amt-2-479-2009, 2009.
- 10 Weingartner, E., Saathoff, H., Schnaiter, M., Streit, N., Bitnar, B. and Baltensperger, U.: Absorption of light by soot particles: determination of the absorption coefficient by means of aethalometers, *J. Aerosol Sci.*, 34(10), 1445–1463, doi:10.1016/S0021-8502(03)00359-8, 2003.
- 15 Zhang, Q., Worsnop, D. R., Canagaratna, M. R. and Jimenez, J. L.: Hydrocarbon-like and oxygenated organic aerosols in Pittsburgh: insights into sources and processes of organic aerosols, *Atmospheric Chem. Phys.*, 5(12), 3289–3311, doi:10.5194/acp-5-3289-2005, 2005.
- 20 Zhang, Q., Jimenez, J. L., Canagaratna, M. R., Allan, J. D., Coe, H., Ulbrich, I., Alfarra, M. R., Takami, A., Middlebrook, A. M., Sun, Y. L., Dzepina, K., Dunlea, E., Docherty, K., DeCarlo, P. F., Salcedo, D., Onasch, T., Jayne, J. T., Miyoshi, T., Shimojo, A., Hatakeyama, S., Takegawa, N., Kondo, Y., Schneider, J., Drewnick, F., Borrmann, S., Weimer, S., Demerjian, K., Williams, P., Bower, K., Bahreini, R., Cottrell, L., Griffin, R. J., Rautiainen, J., Sun, J. Y., Zhang, Y. M. and Worsnop, D. R.: Ubiquity and dominance of oxygenated species in organic aerosols in anthropogenically-influenced Northern Hemisphere midlatitudes, *Geophys. Res. Lett.*, 34(13), L13801, doi:10.1029/2007GL029979, 2007.
- 25 Zhang, S., Riffault, V., Dusanter, S., Augustin, P., Fourmentin, M. and Delbarre, H.: One year of real-time chemical speciation measurements of submicron particulate matter (PM<sub>1</sub>) at a French coastal site: assessment of industrial and shipping emissions, in prep, n.d.
- Zhang, Y., Wang, X., Chen, H., Yang, X., Chen, J. and Allen, J. O.: Source apportionment of lead-containing aerosol particles in Shanghai using single particle mass spectrometry, *Chemosphere*, 74(4), 501–507, doi:10.1016/j.chemosphere.2008.10.004, 2009.

**Table 1. Averaged NR-PM<sub>1</sub> concentrations (in  $\mu\text{g m}^{-3}$ ) - with maximum in parentheses when available - and respective contributions of NR compounds for this study compared to other ACSM campaigns from different locations.**

NR-PM <sub>1</sub> avg ( $\mu\text{g m}^{-3}$ )	Relative contributions (%)					Period	Location	Type of site	Reference
	OM	SO <sub>4</sub>	NO <sub>3</sub>	NH <sub>4</sub>	Chl				
50.0	40	18	25	16	<1	Jun. - Aug. 2011	Beijing (China)	Urban	Sun et al. (2012)
25.9	58	23	7	11	<1	Sept.-Dec. 2015	Hong Kong (China)	Urban	Sun et al. (2016)
15.7 (80)	~44	~6	~38	~11	~1	Jan. - Mar. 2012	Paris (France)	Suburban	Petit et al. (2014)
15.3	72	15	6	8	< 1	Summer - Fall 2011	Atlanta (USA)	Urban	Budisulistiorini et al. (2014)
14.2	58	12	21	8	1	Mar. 2013 – Mar 2014	Ispra (Italy)	Rural background	Bressi et al. (2016)
10.8 (~75)	45	30	11	13	1	Sept. - Oct. 2013	Menyuan, Tibetan Plateau (China)	Rural	Du et al. (2015)
9	31	12	41	14	2	Jul. 2012 -Jun. 2013	Cabauw (The Netherlands)	Rural	Schlag et al. (2015)
7.5 (89)	48	32	7	13	<1	Sept. 2010 - Aug. 2011	Welgegund (South Africa)	Rural	Tiitta et al. (2014)
7.2	52	29	7	12	< 1	Jul. - Sept 2010	New-York (USA)	Urban	Ng et al. (2011)
7.0	57	12	21	9	< 1	Nov. 2010 - Jun. 2012	Southern Great plains (USA)	Rural	Parworth et al. (2015)
~7.0	54	19	11	11	< 5	Jun. 2012 - Jul. 2013	Montseny (Spain)	Rural	Minguillón et al. (2015)
5.4 (68.3)	39	35	9	15	<1	Mar. - Jun. 2015	M'Bour (Senegal)	Suburban	This study
4.9	53	25	7	12	< 1	Jul. 2011 - Apr. 2012	Montsec (Spain)	Rural	Ripoll et al. (2015)
0.3 (9.6)	43	30	7	17	/	Oct. 2012 - Oct. 2013	Jungfraujoch (Switzerland)	Rural	Fröhlich et al. (2015)



**Figure1.** (top left) Dakar and M'Bour locations with city delimitations in orange and (top right) local sources located around the IRD sampling site (red star), with open waste burning areas (green circles), fish-smoking sites (blue triangles) and the M'Bour port (light blue diamond). (bottom) Photographs of (from left to right) smoldering fire in the Gandigal open waste burning area; flaming fire in the Saly Douté open waste burning area; fish-smoking location (drying stage) in the suburb of M'Bour.

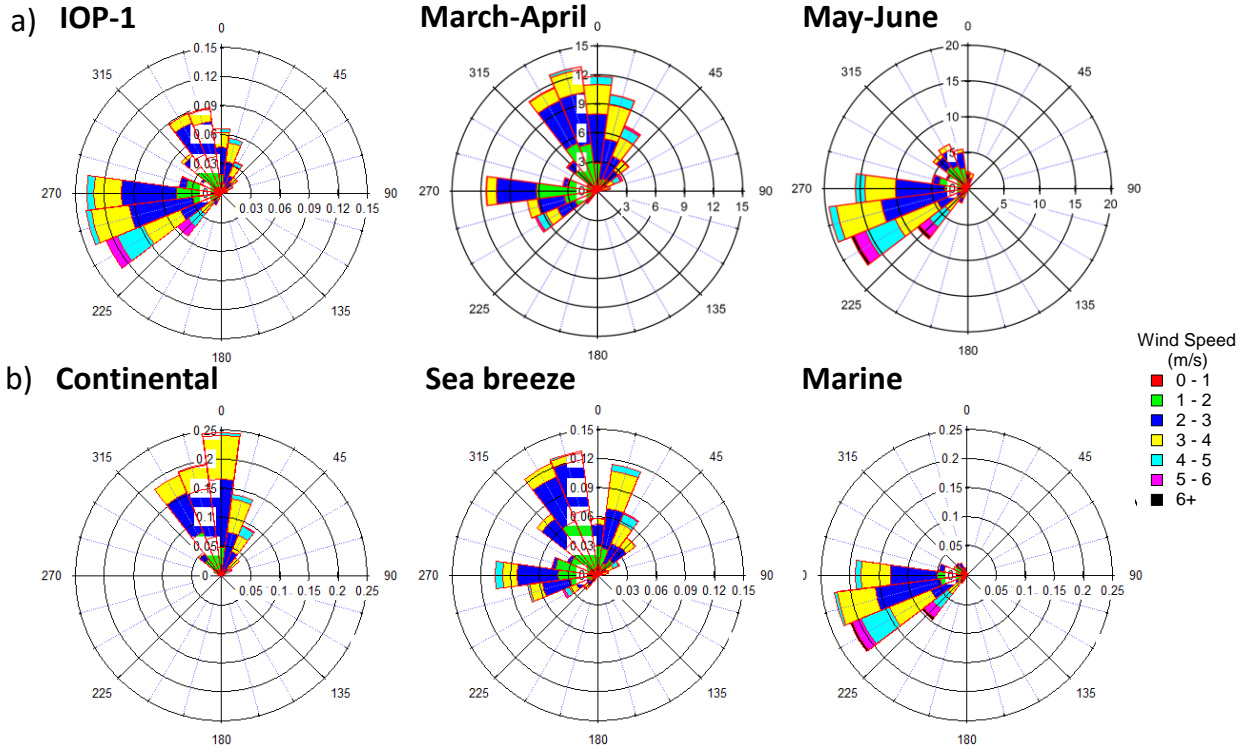


**Fig. 2. Rose plots of wind direction divided into 15° sectors and averaged on 30 minutes (ACSM time step) with wind frequencies as radius (in %) and colored by wind speed intervals measured in M'Bour for (a) the whole dataset and dry and wet months, (b) days classified as continental ( $n = 17$ ), sea breeze ( $n = 29$ ) and marine ( $n = 45$ ).**



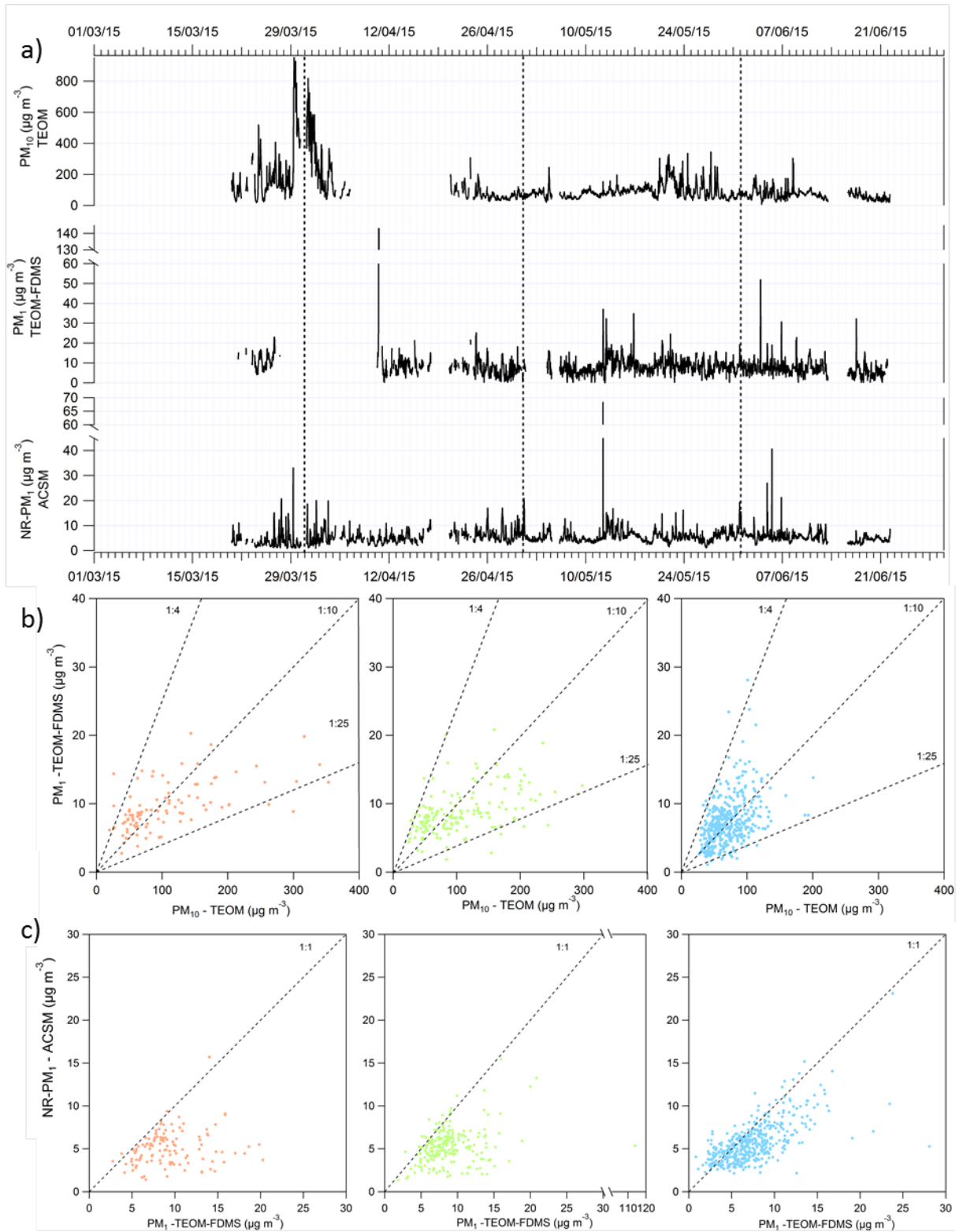
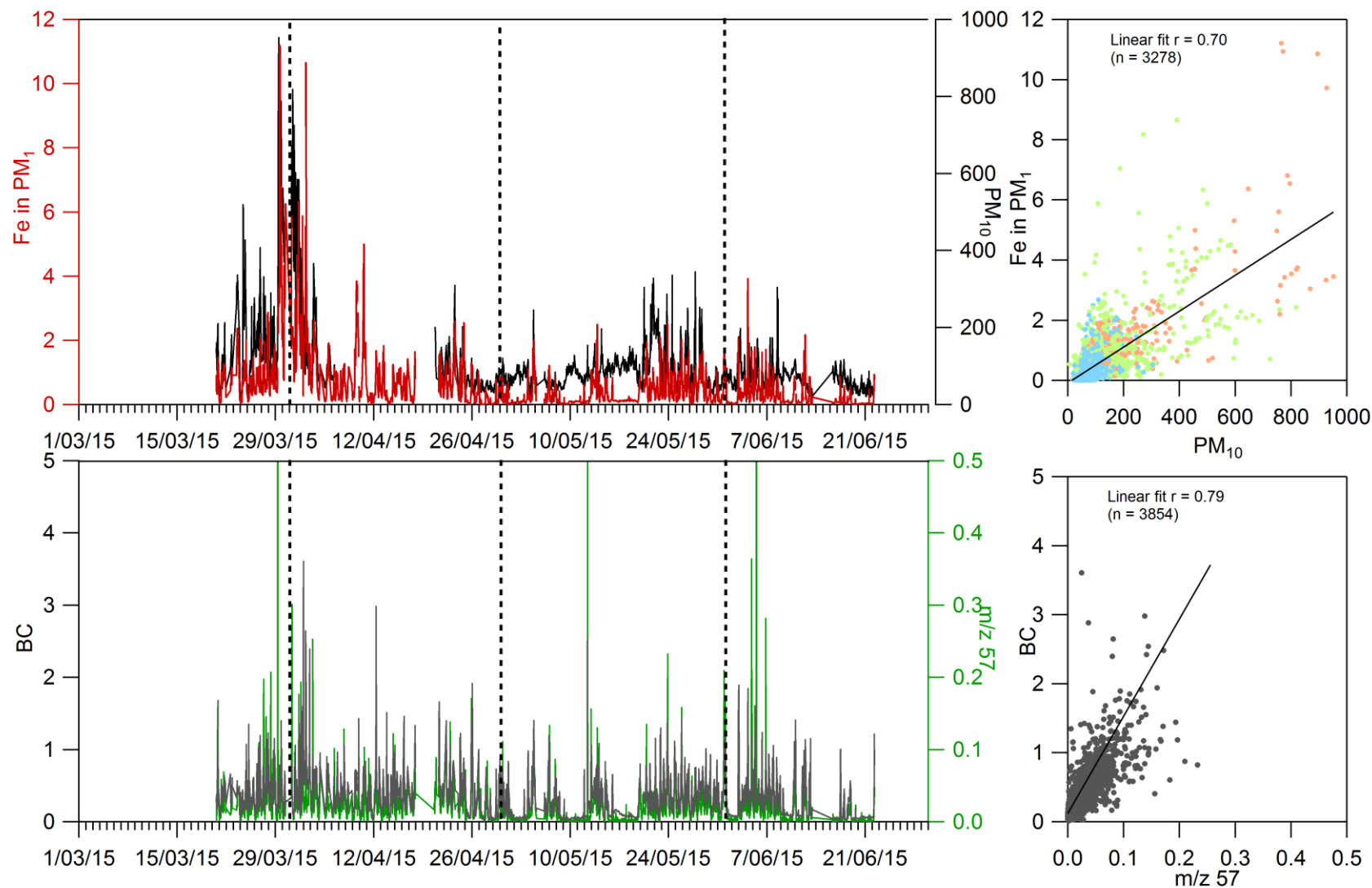
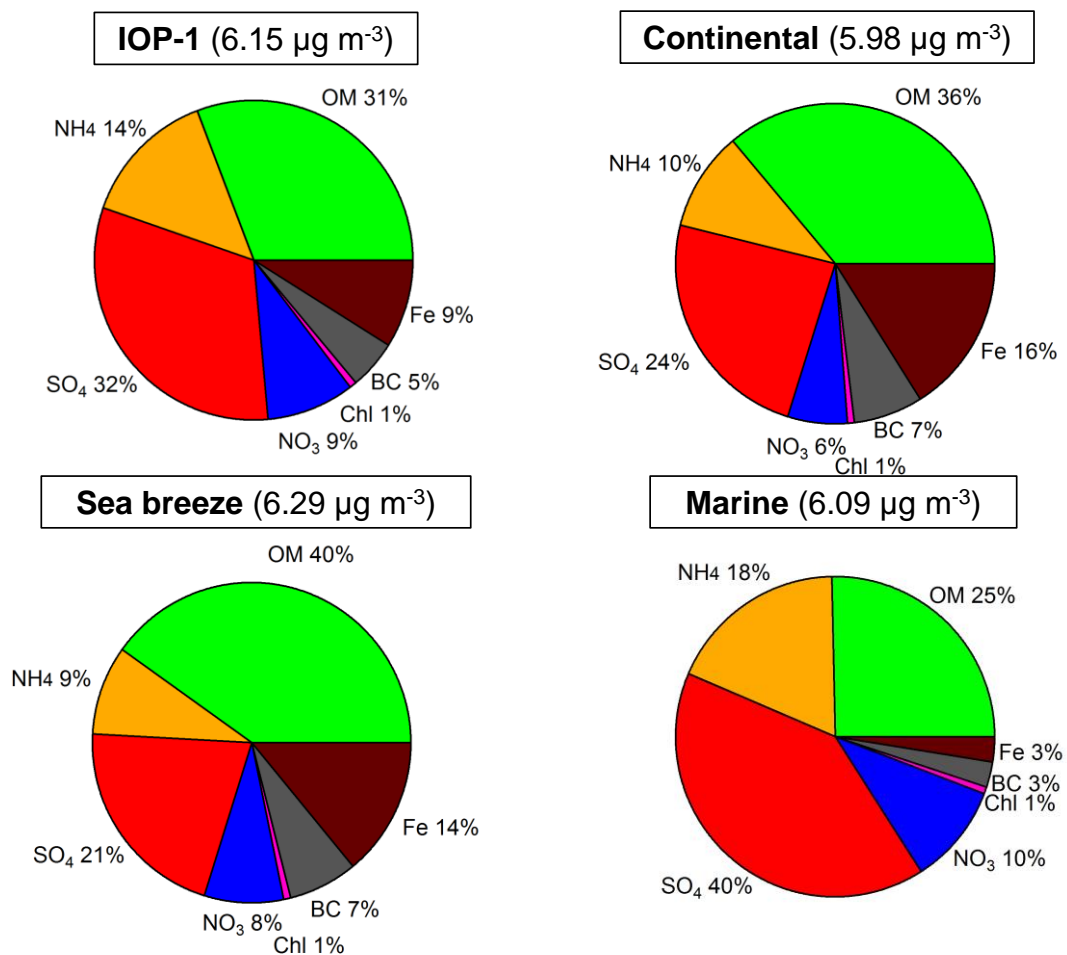


Fig. 3. (a)  $NR-PM_1$ , total  $PM_1$  and  $PM_{10}$  time series (30-minute averages) measured over IOP-1, (b) 2h averaged scatter plots of total  $PM_1$  vs  $PM_{10}$  and (c)  $NR-PM_1$  vs  $PM_1$  for (left) continental, (middle) sea breeze and (right) marine days (dotted lines are visual markers representing ratios between the different variables).



**Fig. 4.** (Left) Time series of (top) Fe and PM<sub>10</sub> concentrations (in  $\mu\text{g m}^{-3}$ ) and (bottom) BC concentration (in  $\mu\text{g m}^{-3}$ ) and m/z 57 (ng m<sup>-3</sup>) 30 min average. (Right) Corresponding scatter plots and their respective linear fits with Fe and PM<sub>10</sub> data colored in red for continental, green for sea breeze and blue for marine days and BC and m/z 57 in grey dots.



**Fig. 5.** Averaged contributions of NR-PM<sub>1</sub>, BC and Fe for IOP-1 (n = 3771), continental (n = 307), sea breeze (n = 799) and marine days (n = 1843) (with average total concentration in  $\mu\text{g m}^{-3}$  in parenthesis).

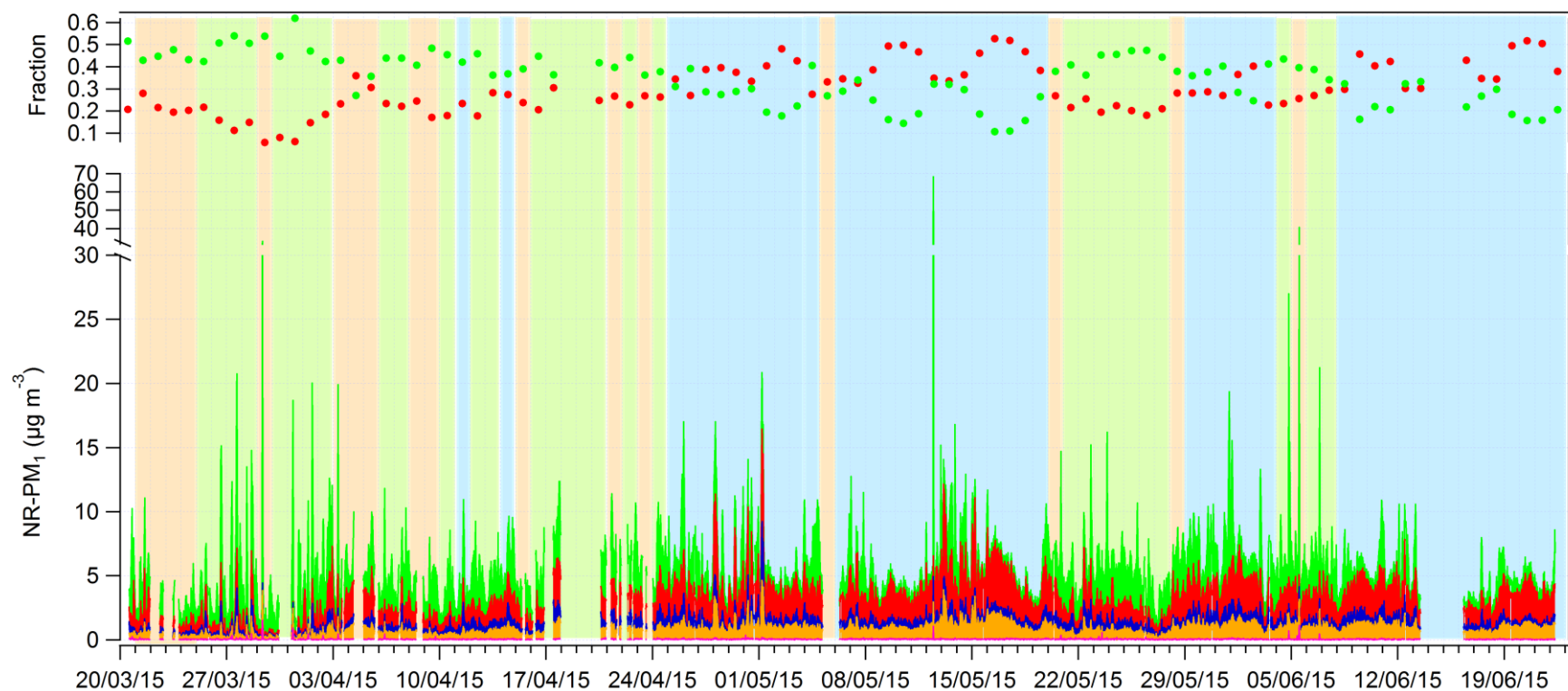


Fig. 6. (Bottom) IOP-1 stacked time series of OM (green), SO<sub>4</sub> (red), NO<sub>3</sub> (blue), NH<sub>4</sub> (orange) and Chl (pink) on ACSM time step (30 min) and (top) daily averaged fraction of OM and SO<sub>4</sub>. Tinted areas correspond to continental days in light pink, sea breeze days in light green and marine days in light blue.

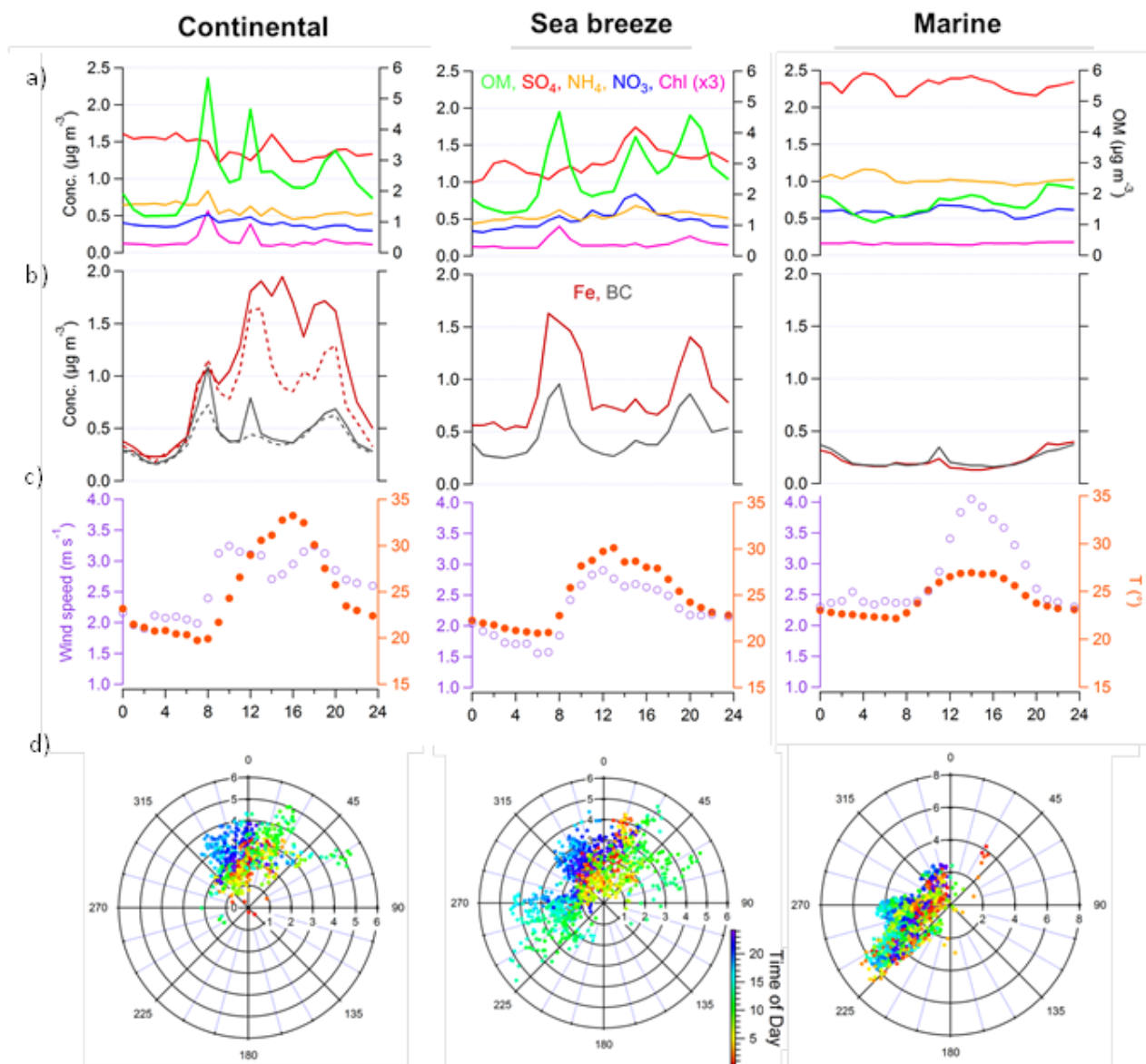
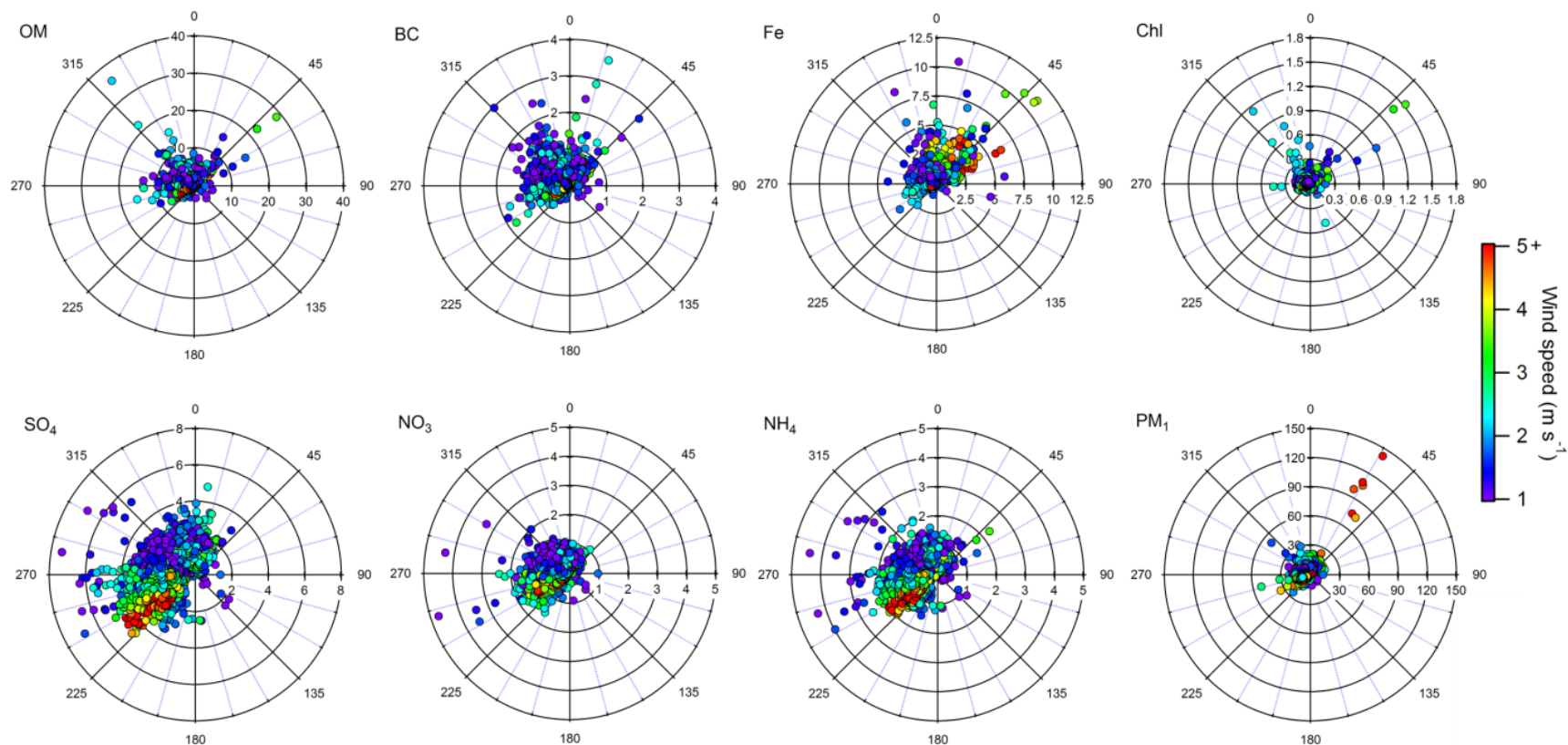
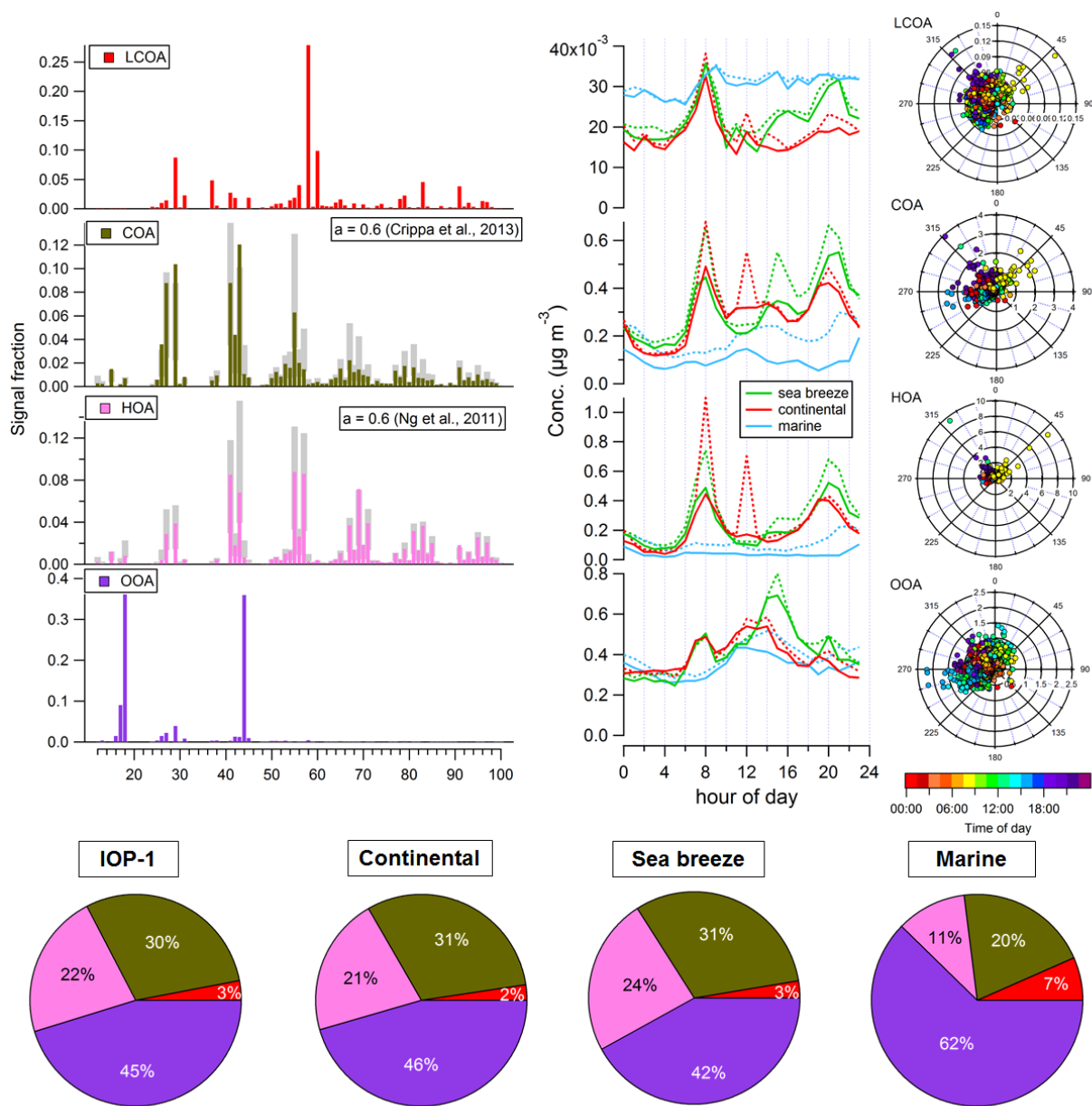


Fig.7. Average daily profiles of (a) NR-PM<sub>1</sub>, (b) BC and Fe concentrations, (c) wind speed and temperature for (from left to right) continental (dotted lines: medians), sea breeze and marine days. (d) Associated wind roses (radius, wind speed in  $\text{m s}^{-1}$ ) colored by time of day in UTC.



**Fig. 8.** Pollution rose plots of OM, BC, Chl, Fe,  $\text{SO}_4$ ,  $\text{NO}_3$ ,  $\text{NH}_4$  and total  $\text{PM}_{10}$  for the whole IOP-1, with concentrations ( $\mu\text{g m}^{-3}$ ) as radius and colored by wind speed (measurements inferior to  $1 \text{ m s}^{-1}$  in grey).





**Fig. 9. PMF constrained 4-factor solution: (left) factor profiles of LCOA, COA, HOA (the two latter constrained), OOA; (middle) corresponding daily cycles according to day types (solid lines: median; dotted lines: average); and (right) pollution rose plots colored by time of day. (bottom) Average pie charts of the contributions to the total organic fraction for IOP-1, continental, sea breeze and marine days.**